Received September 25, 2021, accepted October 14, 2021, date of publication October 19, 2021, date of current version October 29, 2021.

Digital Object Identifier 10.1109/ACCESS.2021.3121428

A New 4-D Multi-Stable Hyperchaotic System With No Balance Point: Bifurcation Analysis, Circuit Simulation, FPGA Realization and Image Cryptosystem

SUNDARAPANDIAN VAIDYANATHAN[1], ACENG SAMBAS[2], ESTEBAN TLELO-CUAUTLE[3], AHMED A. ABD EL-LATIF[4], BASSEM ABD-EL-ATTY[5], OMAR GUILLÉN-FERNÁNDEZ[3], KHALED BENKOUIDER[6], MOHAMAD AFENDEE MOHAMED[7], (Associate Member, IEEE), MUSTAFA MAMAT[7], AND MOHD ASRUL HERY IBRAHIM[8]

[1]School of Electrical and Communication Engineering, Vel Tech University, Avadi, Chennai, Tamil Nadu 600062, India
[2]Department of Mechanical Engineering, Universitas Muhammadiyah Tasikmalaya, Tasikmalaya, Jawa Barat 46196, Indonesia
[3]Department of Electronics, Instituto Nacional de Astrofísica, Óptica y Electrónica (INAOE), Tonantzintla, Puebla 72840, México
[4]Department of Mathematics and Computer Science, Faculty of Science, Menoufia University, Shibin Al Kawm 32511, Egypt
[5]Department of Computer Science, Faculty of Computers and Information, Luxor University, Luxor 85957, Egypt
[6]Non Destructive Testing Laboratory, Automatic Department, University of Jijel, Jijel 18000, Algeria
[7]Faculty of Informatics and Computing, Universiti Sultan Zainal Abidin (UniSZA), Kuala Terengganu 21300, Malaysia
[8]Faculty of Entrepreneurship and Business, Universiti Malaysia Kelantan, Kota Bharu Kelantan 16100, Malaysia

Corresponding author: Mohamad Afendee Mohamed (mafendee@unisza.edu.my)

This work was supported by the Center for Research Excellence, Incubation Management Center, Universiti Sultan Zainal Abidin, Malaysia.

ABSTRACT In this work, we describe the model of a new 4-D hyperchaotic system with no balance point and deduce that the new hyperchaotic system has a hidden attractor. We present a detailed bifurcation analysis for the new hyperchaotic dynamo system with respect to the system parameters and also exhibit that the new hyperchaotic system displays multistability with coexisting attractors. Using NI Multisim 14.0, we design an electronic circuit for the implementation of the new 4-D hyperchaotic system and present the circuit simulation results. We also show the implementation of the new 4-D hyperchaotic system by using a field programmable gate array (FPGA). The hardware resources are reduced by designing single-constant multipliers, adders, subtractors and multipliers. The FPGA design is done for three numerical methods, namely: Forward-Euler, Backward-Euler and fourth-order Runge-Kutta. We demonstrate that experimental chaotic attractors are in good agreement with theoretical simulations. To verify the ability of the presented hyperchaotic system for designing robust cryptosystems, we suggest a novel image cryptosystem using the proposed hyperchaotic system. Simulation outcomes confirm the effectiveness of the proposed image cryptosystem, and consequently, the effectiveness of the proposed 4-D hyperchaotic system in designing diverse cryptographic purposes.

INDEX TERMS Hyperchaotic systems, hyperchaos, multi-stability, bifurcations, Lyapunov exponents, circuit simulation, FPGA, numerical methods, image encryption.

I. INTRODUCTION

Hyperchaos theory deals with hyperchaotic dynamical systems and has several applications in engineering due to the high complexity of hyperchaotic dynamical systems equipped with two or more positive Lyapunov characteristic exponents.

The associate editor coordinating the review of this manuscript and approving it for publication was Di He.

Bonatto [1] observed hyperchaotic behavior of light polarization states in the output of a free-running laser diode. Barakat *et al.* [2] obtained a hyperchaotic attractor from a two-photon laser with multi-intermediate states. Petavratzis *et al.* [3] described a new enhanced technique for the motion control of a mobile robot using a hyperchaotic system dynamics as chaotic path generator for the mobile robot. Vaidyanathan *et al.* [4] reported a hyperchaotic mechanical system exhibiting Hopf bifurcations and discussed its

circuit simulations. Luo *et al.* [5] reported the circuit design and control of a memristor-based hyperchaotic system. Zhang *al.* [6] proposed a new symmetric image encryption method using a hyperchaotic system, Arnold transform and phase-truncated fractional Fourier transform. Bian and Yu [7] proposed a new cryptosystem for communication using a new 6-D hyperchaotic system.

Bifurcation analysis for a hyperchaotic system deals with the dynamic analysis of the system with respect to changes in the various parameters [8]–[11]. For a hyperchaotic system, multistability refers to the coexistence of two or more attractors of the system for the same values of the parameters but differing values of the initial states [12]–[14].

This work proposes a new 4-D hyperchaotic system with no balance point. Such systems are known to have hidden attractors. In Section II, we state a dynamic model of the new system and show that it has no balance point. We also observe that the new 4-D hyperchaotic system has rotational symmetry about the third coordinate axis. In Section III, we present a detailed bifurcation analysis of the new hyperchaotic system presented in this work and also exhibit that it has multistability with coexisting attractors.

Circuit design of chaotic and hyperchaotic systems is very important for practical applications [15]–[17]. Mobayen *et al.* [18] discussed a family of chameleon chaotic systems with quadratic nonlinearities and designed an electronic circuit for a chameleon chaotic system. Petrzela [19] carried out an experimental verification of a new hyperchaotic system based on a two-stage amplifier. In Section V, we present the design of an electronic circuit of the new hyperchaotic system via NI Multisim 14.0, and describe its circuit simulations.

It has been shown that any chaotic system can be implemented by using field-programmable gate arrays (FPGAs) [20], this is due to the advantage of fast verification and reconfigurability of the device. Once the mathematical model is given, one must consider the use of different numerical methods [21] to proceed to the FPGA implementation, and also, one can reduce hardware resources by designing single-constant multipliers [22], adders, subtractors and multipliers. In this work, FPGA design of the new 4-D hyper-chaotic system is performed by applying three numerical methods, namely: Forward-Euler, Backward-Euler and fourth-order Runge-Kutta numerical methods.

In Section VI, we demonstrate that experimental chaotic attractors are in good agreement with theoretical simulations, and also provide hardware resources for different numerical methods.

Information security acts a vital purpose in our daily lives [23]. Digital images exemplify the common model of data description. Image data can be secured via utilizing one of the image cryptosystems [24]–[28] or using one of the image data hiding methods [29], [30].

In Section VII, we propose a new image encryption mechanism based on the new hyperchaotic system. In our image cryptosystem, the hash code for the pristine image is calculated at first and utilizes this hash code for updating the primary conditions of the presented hyperchaotic system to guarantee pristine image sensitivity. The output of iterating the hyperchaotic system is four chaotic sequences in which the last chaotic sequence is utilized for constructing a new sequence from the other first three sequences, and the pristine image is permutated then substituted utilizing the new sequence. Simulation outputs confirm the effectiveness of the proposed image cryptosystem.

II. A NEW HYPERCHAOTIC SYSTEM WITH NO BALANCE POINT

The dynamical equations of the new 4-D system proposed in this work are given by

$$\begin{cases} \dot{y}_1 = a(y_2 - y_1) - by_2y_3 + y_4 \\ \dot{y}_2 = y_1(1 - cy_3) \\ \dot{y}_3 = y_1y_2 - d \\ \dot{y}_4 = -y_1 - y_2 \end{cases} \tag{1}$$

Eq. (1) represents a 4-D system with the state $Y = (y_1, y_2, y_3, y_4)$ and the system involves three quadratic nonlinearities $y_1\ y_2$, $y_2\ y_3$ and $y_1\ y_3$. We assume that the system constants a, b, c, d are all positive.

By calculating Lyapunov characteristic exponents, it will be shown in this work that the system (1) has a hyperchaotic attractor for the value of constants as

$$a = 0.6,\ b = 0.1,\ c = 25,\ d = 4 \tag{2}$$

For numerical simulations, we take $(a, b, c, d) = (0.6, 0.1, 25, 4)$. We choose the initial state as $Y(0) = (0.6, 0.8, 0.6, 0.8)$. Then the Lyapunov characteristic exponents for the 4-D system (1) were computed for $T = 1E5$ seconds as follows:

$$\begin{aligned} LE_1 &= 0.8367, \quad LE_2 = 0.1642, \\ LE_3 &= 0, \quad LE_4 = -1.6009 \end{aligned} \tag{3}$$

The presence of two positive Lyapunov characteristic exponents in Eq. (3) pinpoints that the 4-D system (1) is *hyperchaotic*.

The Kaplan-Yorke dimension of the 4-D hyperchaotic system (1) is obtained by the following calculation:

$$D_{KY} = 3 + \frac{LE_1 + LE_2 + LE_3}{|LE_4|} = 3.6252 \tag{4}$$

The 4-D system (1) has high complexity since it has a large value of D_{KY}.

We also remark that the hyperchaotic system (1) has rotation symmetry about the y_3-axis since it is invariant under the transformation of coordinates

$$(y_1, y_2, y_3, y_4) \mapsto (-y_1, -y_2, y_3, -y_4) \tag{5}$$

The balance points of the hyperchaotic system (1) are found by solving following algebraic system of equations:

$$a(y_2 - y_1) - by_2y_3 + y_4 = 0 \tag{6a}$$

$$y_1(1-cy_3) = 0 \tag{6b}$$
$$y_1y_2-d = 0 \tag{6c}$$
$$-y_1 - y_2 = 0 \tag{6d}$$

From Eq. (6d), we get

$$y_2 = -y_1 \tag{7}$$

Substituting $y_2 = -y_1$ into Eq. (6c), we get

$$y_1^2 + d = 0 \tag{8}$$

which admits no real solution since $d > 0$.

Hence, we conclude that the 4-D hyperchaotic system (1) does not have any balance point. Thus, the hyperchaotic system (1) belongs to the class of systems with hidden attractors [31]–[33].

The 2D signal plots of the 4-D hyperchaotic system (1) for the constants $(a, b, c, d) = (0.6, 0.1, 25, 4)$ and the initial state $Y(0) = (0.6, 0.8, 0.6, 0.8)$ are depicted in Figure 1.

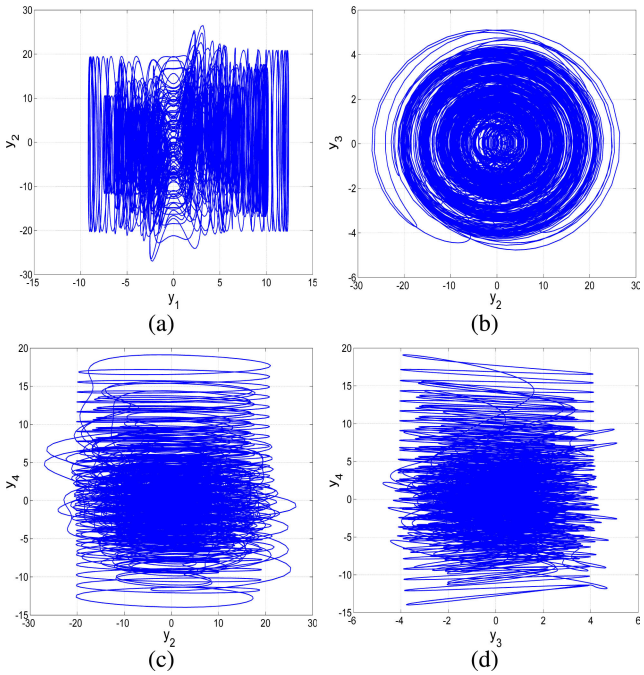

FIGURE 1. 2-D signal plots of the 4-D hyperchaotic system (1) for $(a, b, c, d) = (0.6, 0.1, 25, 4)$ and the initial state $Y(0) = (0.6, 0.8, 0.6, 0.8)$: (a) (y_1, y_2) plane, (b) (y_2, y_3) plane, (c) (y_2, y_4) plane and (d) (y_3, y_4) plane.

III. BIFURCATION ANALYSIS AND MULTISTABILITY OF THE NEW HYPERCHAOTIC SYSTEM

Lyapunov exponents spectrum and bifurcation diagram represent the two most important tools to analyse the dynamical behavior of a system. Furthermore, the Kaplan-Yorke fractal dimension is an effective index of system complexity. In this section, dynamical behavior and complexity of the new 4-D hyperchaotic system (1) are investigated by using numerical calculations with the positive parameters a, b, c and d varying.

A. PARAMETER A VARYING

Here, we fix the values of the system parameters as

$$b = 0.1, \quad c = 25, \quad d = 4 \tag{9}$$

and vary the parameter a.

Lyapunov exponents spectrum and the corresponding bifurcation diagram of system (1) when a takes values in the interval $[0.5, 5]$ are depicted in Figure 2. We can see a good agreement between the bifurcation diagram and the Lyapunov exponents spectrum.

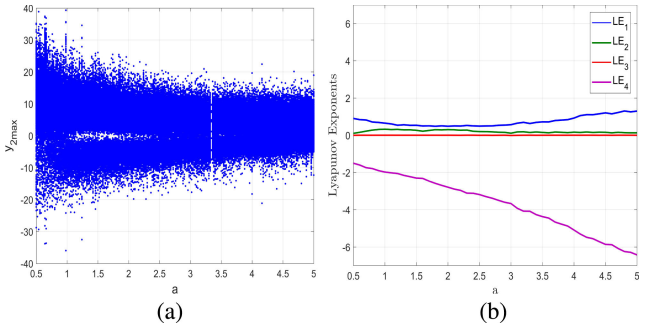

FIGURE 2. Bifurcation diagram (a) and Lyapunov exponents spectrum (b) of the new 4-D hyperchaotic system (1) when $b = 0.1$, $c = 25$, $d = 4$ and $a \in [0.5, 5]$.

It can be seen from Figure 2 that the proposed 4-D system (1) can exhibit hyperchaotic behavior with two positive Lyapunov exponents and different levels of complexity.

When $a = 5$, the new 4-D system (1) generates hyperchaotic behavior. The corresponding Lyapunov exponents are:

$$LE_1 = 1.297, \quad LE_2 = 0.130,$$
$$LE_3 = 0, \quad LE_4 = -6.425 \tag{10}$$

and the corresponding Kaplan-Yorke fractal dimension is equal to $D_{KY} = 3.222$.

When $a = 2$, the new 4-D system (1) generates hyperchaotic behaviour. The corresponding Lyapunov exponents are:

$$LE_1 = 0.484, \quad LE_2 = 0.305,$$
$$LE_3 = 0, LE_4 = -2.710 \tag{11}$$

and the corresponding Kaplan-Yorke fractal dimension is equal to $D_{KY} = 3.291$ which indicates more complexity of the hyperchaotic attractor.

When $a = 0.5$, The Lyapunov exponents are:

$$LE_1 = 0.902, \quad LE_2 = 0.103,$$
$$LE_3 = 0, \quad LE_4 = -1.501 \tag{12}$$

and the corresponding Kaplan-Yorke fractal dimension equal to $D_{KY} = 3.670$, which is the highest value obtained for the new system (1) when a varies in $[0.5, 5]$, indicating extreme complexity of the dynamics.

TABLE 1. Dynamics, Lyapunov exponents and Kaplan-Yorke dimension of the 4-D system (1) versus its parameters.

Dynamics	Parameters				Bifurcation Parameter	Lyapunov Exponents				D_{KY}	Attractor
	a	b	c	d		LE_1	LE_2	LE_3	LE_4		
Periodic	$[1, 1.6]$	1.5	25	10	$a = 1$	0	-0.067	-0.465	-0.475	0	Figure 5 (a)
	1	$[0.85, 2]$	25	10	$b = 1.9$	0	-0.092	-0.454	-0.457	0	Figure 9 (a)
	1	0.8	20	$[3.8, 4]$, $[4.4, 4.7]$, $[4.9, 5]$	$d = 4.7$	0	-0.069	-0.455	-0.478	0	Figure 15 (a)
Chaos	$[1.6, 5.7]$	1.5	25	10	$a = 3$	0.124	0	-0.066	-3.065	3.019	Figure 4 (b)
	1	$[0.5, 0.85]$	25	10	$b = 0.8$	0.031	0	-0.327	-0.709	2.095	Figure 9 (b)
	0.6	0.1	$[3, 10]$	4	$c = 4$	0.625	0	-0.048	-1.178	3.489	Figure 11 (a)
	0.6	0.1	25	$[-5, 0]$	$d = 0.1$	0.575	0	-0.011	-1.166	3.484	Figure 13 (a)
	1	0.8	20	$[0, 0.6]$, $[3, 3.8]$, $[4, 4.4]$, $[4.7, 4.9]$	$d = 0.2$	0.382	0	-0.018	-1.275	3.215	Figure 15 (b)
Hyperchaos	$[0.5, 5]$	0.1	25	4	$a = 2$	0.902	0.103	0	-1.501	3.670	Figure 3 (c)
	$[5.7, 10]$	1.5	25	10	$a = 9$	2.030	0.072	0	-11.101	3.189	Figure 5 (c)
	0.6	$[0, 0.25]$	25	4	$b = 0$	1.026	0.126	0	-1.744	3.661	Figure 7 (c)
	1	$[0, 0.5]$	25	10	$b = 0.1$	0.503	0.196	0	-1.698	3.412	Figure 9 (c)
	0.6	0.1	$[10, 30]$	4	$c = 30$	0.850	0.201	0	-1.651	3.637	Figure 11 (b)
	0.6	0.1	25	$[0, 15]$	$d = 15$	0.573	0.259	0	-1.432	3.581	Figure 14 (b)
	1	0.8	20	$[0.6, 3]$	$d = 2$	0.455	0.173	0	-1.625	3.386	Figure 15 (c)

Various phase portraits of the new 4-D system (1) for parameters values as in (9) and different values of a are given in Figure 3.

Now, in order to identify the other types of behaviour of the 4-D system (1) when the bifurcation parameter a varies, we plot the bifurcation diagram for other values of the constant parameters b, c and d.

We fix the values of the parameters as

$$b = 1.5, \quad c = 25, \quad d = 10 \tag{13}$$

and vary the parameter a.

Lyapunov exponents spectrum and the corresponding bifurcation diagram of system (1) when a takes values in the interval[1, 10] are depicted in Figure 4. We can see a good agreement between the bifurcation diagram and the Lyapunov exponents spectrum. Figure 4 shows that the proposed 4-D system (1) can exhibit periodic behavior, chaotic behavior and hyperchaotic behavior.

When $a \in [1, 1.6]$, the new 4-D system (1) exhibits periodic behavior with no complexity. When $a \in [1.6, 5.7]$, system (1) exhibits chaotic behavior with one positive Lyapunov exponent. When $a \in [5.7, 10]$, the new 4-D system (1) exhibits hyperchaotic behavior with two positive Lyapunov exponents and high complexity.

Various phase portraits of the new 4-D system (1) for parameters values as in (13) and different values of a are given in Figure 3.

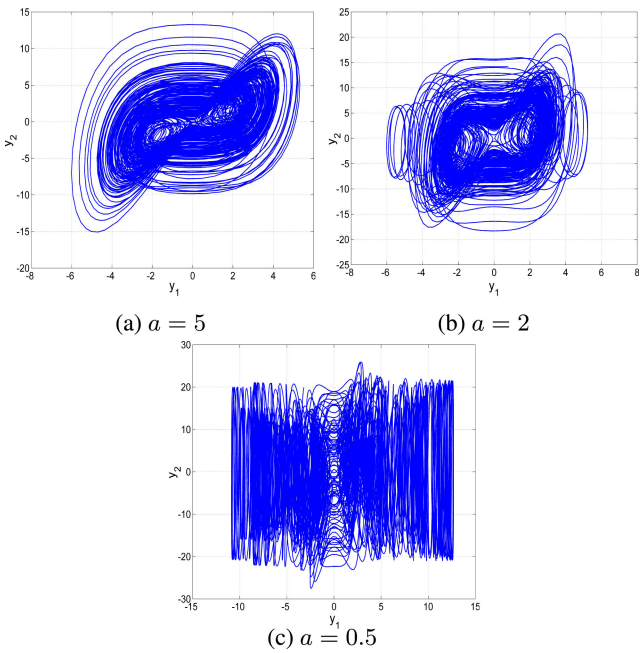

(a) $a = 5$ (b) $a = 2$

(c) $a = 0.5$

FIGURE 3. 2-D plot of the new 4-D hyperchaotic system (1) in the (y_1, y_2) -plane for $b = 0.1$, $c = 25$, $d = 4$ and different values of a.

In addition, Table 1 gives dynamics, Lyapunov exponents and Kaplan-Yorke fractal dimension of the proposed 4-D system (1) for different values of a.

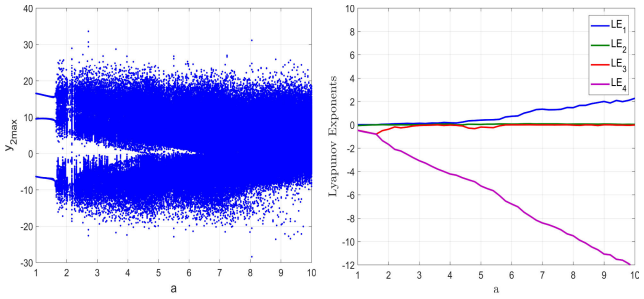

(a) (b)

FIGURE 4. Bifurcation diagram (a) and Lyapunov exponents spectrum (b) of the new 4-D hyperchaotic system (1) when $b = 1.5$, $c = 25$, $d = 10$ and $a \in [1, 10]$.

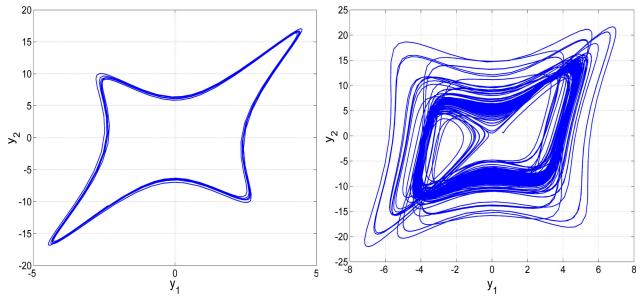

(a) $a = 1$ (b) $a = 3$

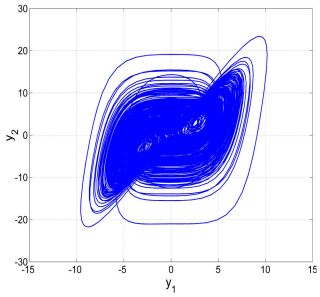

(c) $a = 9$

FIGURE 5. 2-D plot of the new 4-D hyperchaotic system (1) in the (y_1, y_2) -plane for $b = 1.5$, $c = 25$, $d = 10$ and different values of a: (a) Periodic attractor ($a = 1$), (b) Chaotic attractor ($a = 3$) and (c) Hyperchaotic attractor ($a = 9$).

B. PARAMETER B VARYING

Here, we fix the values of the system parameters as

$$a = 0.6, \quad c = 25, \quad d = 4 \tag{14}$$

and vary the parameter b.

Lyapunov exponents spectrum and the corresponding bifurcation diagram of system (1) when b takes values in the interval [0, 0.25] are depicted in Figure 6. We can see a good agreement between the bifurcation diagram and the Lyapunov exponents spectrum.

It can be seen from Figure 6 that the proposed 4-D system (1) can exhibit hyperchaotic behavior with two positive Lyapunov exponents and different levels of complexity.

When $b = 0.15$, the new 4-D system (1) generates hyperchaotic behavior. The corresponding Lyapunov exponents are:

$$LE_1 = 0.725, \quad LE_2 = 0.205,$$
$$LE_3 = 0, \quad LE_4 = -1.526 \tag{15}$$

and the corresponding Kaplan-Yorke fractal dimension is equal to $D_{KY} = 3.609$.

When $b = 0.12$, the new 4-D system (1) generates hyperchaotic behaviour. The corresponding Lyapunov exponents are:

$$LE_1 = 0.819, \quad LE_2 = 0.214,$$
$$LE_3 = 0, \quad LE_4 = -1.633 \tag{16}$$

and the corresponding Kaplan-Yorke fractal dimension is equal to $D_{KY} = 3.633$ which indicates more complexity of the hyperchaotic attractor.

When $b = 0$, The Lyapunov exponents are:

$$LE_1 = 1.026, \quad LE_2 = 0.126,$$
$$LE_3 = 0, \quad LE_4 = -1.744 \tag{17}$$

and the corresponding Kaplan-Yorke fractal dimension equal to $D_{KY} = 3.661$, which is the highest value obtained for the new system (1) when b varies in [0, 0.25], indicating extreme complexity of the dynamics.

Various phase portraits of the new 4-D system (1) for parameters values as in (14) and different values of b are given in Figure 7.

Now, in order to identify the other types of behaviour of the 4-D system (1) when the bifurcation parameter b varies, we plot the bifurcation diagram for other values of the constant parameters a, c and d.

We fix the values of the parameters as

$$a = 1, \quad c = 25, \quad d = 10 \tag{18}$$

and vary the parameter b.

Lyapunov exponents spectrum and the corresponding bifurcation diagram of system (1) when b takes values in the interval[0, 2] are depicted in Figure 8. We can see a good agreement between the bifurcation diagram and the Lyapunov exponents spectrum. Figure 8 shows that the proposed 4-D system (1) can exhibit periodic behavior, chaotic behavior and hyperchaotic behavior.

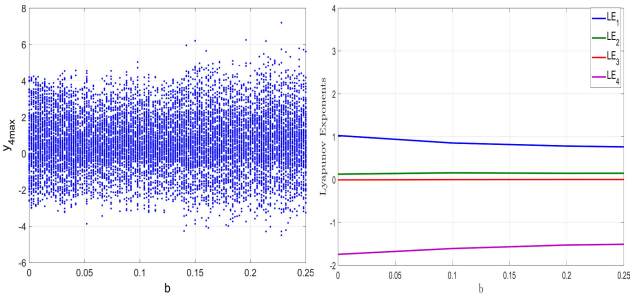

(a) (b)

FIGURE 6. Bifurcation diagram (a) and Lyapunov exponents spectrum (b) of the new 4-D hyperchaotic system (1) when $a = 0.6$, $c = 25$, $d = 4$ and $b \in [0, 0.25]$.

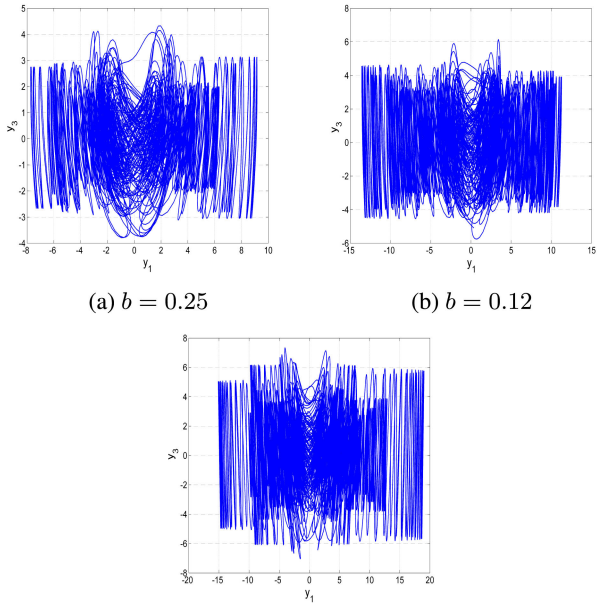

(a) $b = 0.25$ (b) $b = 0.12$

(c) $b = 0$

FIGURE 7. 2-D plots of the new 4-D hyperchaotic system (1) in the (y_1, y_3) -plane for $a = 0.6$, $c = 25$, $d = 4$ and different values of b.

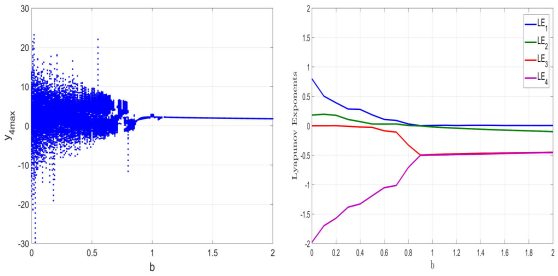

(a) (b)

FIGURE 8. Bifurcation diagram (a) and Lyapunov exponents spectrum (b) of the new 4-D hyperchaotic system (1) when $b = 1.5$, $c = 25$, $d = 10$ and $a \in [1, 10]$.

When $b \in [0, 0.5]$, the new 4-D system (1) exhibits two positive Lyapunov exponents and high value of fractal dimension. When $b \in [0.5, 0.85]$, the system (1) exhibits chaotic behavior with one positive Lyapunov exponent. When $b \in [0.85, 2]$, the new 4-D system (1) exhibits periodic behavior with no complexity.

Various phase portraits of the new 4-D system (1) for parameters values as in (18) and different values of a are given in Figure 7.

In addition, Table 1 gives dynamics, Lyapunov exponents and Kaplan-Yorke fractal dimension of the proposed 4-D system (1) for different values of b.

C. PARAMETER C VARYING

Here, we fix the values of the system parameters as

$$a = 0.6, \quad b = 0.1, \quad d = 4 \tag{19}$$

and vary the parameter c.

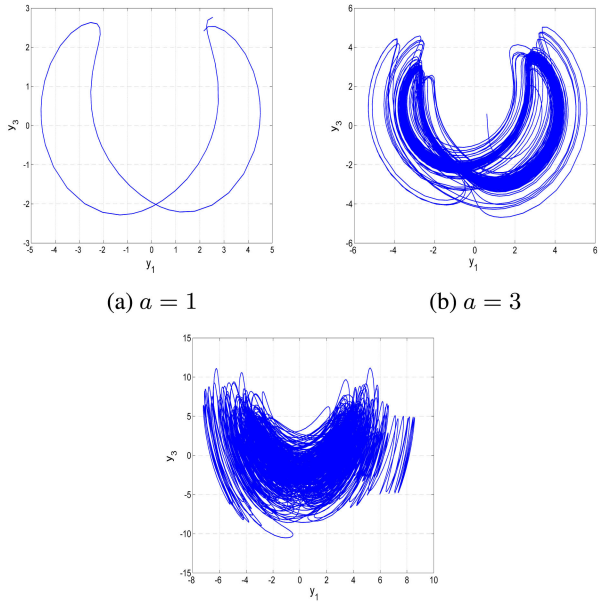

(a) $a = 1$ (b) $a = 3$

(c) $a = 9$

FIGURE 9. 2-D plots of the new 4-D hyperchaotic system (1) in the (y_1, y_3) -plane for $a = 1$, $c = 25$, $d = 10$ and different values of b: (a) Periodic attractor ($b = 1.9$), (b) Chaotic attractor ($b = 0.8$) and (c) Hyperchaotic attractor ($b = 0.1$).

Lyapunov exponents spectrum and the corresponding bifurcation diagram of system (1) when c takes values in the interval $[3, 30]$ are depicted in Figure 10. We can see a good agreement between the bifurcation diagram and the Lyapunov exponents spectrum.

It can be seen from Figure 10 that the proposed 4-D system (1) can exhibit chaotic behavior or hyperchaotic behavior when c varies.

When $c \in [3, 10]$, the new system (1) exhibits chaotic behavior with one positive Lyapunov exponent.

When $c \in [10, 30]$, the new system (1) exhibits hyperchaotic behavior with two positive Lyapunov exponents and high complexity.

Various phase portraits of the new 4-D system (1) for the values of parameters as in (19) and different values of c are given in Figure 11. Also, Table 1 gives dynamics, Lyapunov exponents and Kaplan-Yorke fractal dimension of the system (1) for different values of c.

D. PARAMETER D VARYING

Here, we fix the values of the system parameters as

$$a = 0.6, \quad b = 0.1, \quad c = 25 \tag{20}$$

and vary the parameter d.

Lyapunov exponents spectrum and the corresponding bifurcation diagram of system (1) when d takes values in the interval $[-5, 15]$ are depicted in Figure 12. We can see a good agreement between the bifurcation diagram and the Lyapunov exponents spectrum.

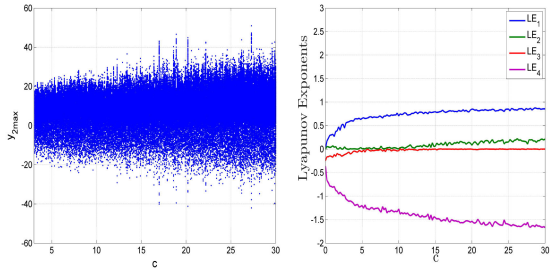

(a) (b)

FIGURE 10. Bifurcation diagram (a) and Lyapunov exponents spectrum (b) of the new 4-D hyperchaotic system (1) when $a = 0.6$, $b = 0.1$, $d = 4$ and $c \in [0, 30]$.

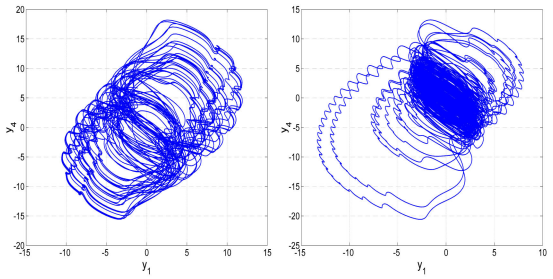

(a) $c = 4$ (b) $c = 30$

FIGURE 11. 2-D plots of the new 4-D hyperchaotic system (1) in the (y_1, y_4) -plane for $a = 0.6$, $b = 0.1$, $d = 10$ and different values of c.

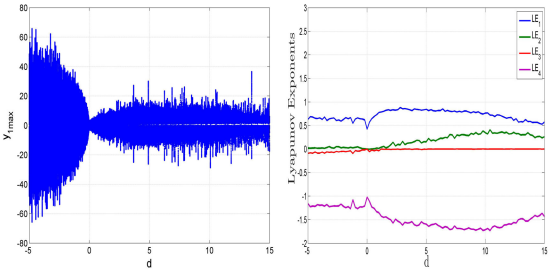

(a) (b)

FIGURE 12. Bifurcation diagram (a) and Lyapunov exponents spectrum (b) of the new 4-D hyperchaotic system (1) when $a = 0.6$, $b = 0.1$, $c = 25$ and $d \in [-5, 15]$.

It can be seen from Figure 12 that the proposed 4-D system (1) can exhibit chaotic behavior or hyperchaotic behavior when d varies.

When $d \in [-5, 0]$, the new system (1) exhibits chaotic behavior with one positive Lyapunov exponent.

When $d \in [0, 15]$, the new system (1) exhibits hyperchaotic behavior with two positive Lyapunov exponents and high complexity.

Various phase portraits of the new 4-D system (1) for the values of parameters as in (20) and different values of d are given in Figure 13.

Now, in order to identify the other behavior of the 4-D system when the bifurcation parameter d varies, we plot the bifurcation diagram for other values of the constant parameters a, b and c.

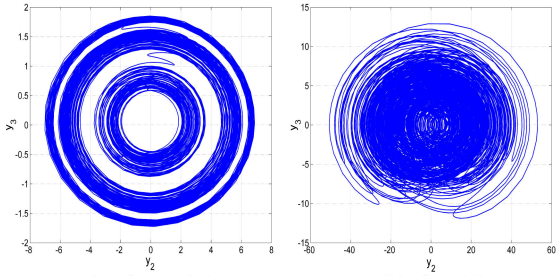

(a) $d = -0.1$ (b) $d = 15$

FIGURE 13. 2-D plots of the new 4-D hyperchaotic system (1) in the (y_2, y_3) -plane for $a = 0.6$, $b = 0.1$, $c = 15$ and different values of d.

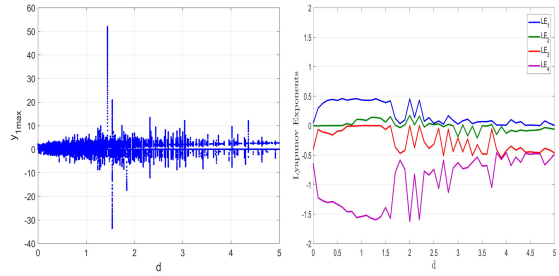

(a) (b)

FIGURE 14. Bifurcation diagram (a) and Lyapunov exponents spectrum (b) of the new 4-D system (1) when $a = 1$, $b = 0.8$, $c = 20$ and $d \in [0, 5]$.

We fix the values of the parameters as

$$a = 1, \quad b = 0.8, \quad c = 20 \tag{21}$$

and vary the parameter d.

Lyapunov exponents spectrum and the corresponding bifurcation diagram of the system (1) when d takes values in the interval $[0, 5]$ are depicted in Figure 14. We can see a good agreement between the bifurcation diagram and the Lyapunov exponents spectrum. Figure 14 shows that the proposed 4-D system can generate periodic behavior, chaotic behavior and hyperchaotic behavior.

We define two sets

$$I = [3.8, 4] \cup [4.4, 4.7] \cup [4.9, 5] \tag{22}$$

and

$$J = [0, 0.6] \cup [3, 3.8] \cup [4, 4.4] \cup [4.7, 4.9] \tag{23}$$

When $d \in I$, the new 4-D system (1) exhibits periodic behavior with no complexity.

When $d \in J$, the new 4-D system (1) exhibits chaotic behavior with one positive Lyapunov exponent.

When $d \in [0.6, 3]$, the new 4-D system (1) exhibits hyperchaotic behavior with two positive Lyapunov exponents.

Various phase portraits of the new 4-D system (1) for the values of parameters as in (21) and different values of d are given in Figure 15. Also, Table 1 gives dynamics, Lyapunov exponents and Kaplan-Yorke fractal dimension of the system (1) for different values of d.

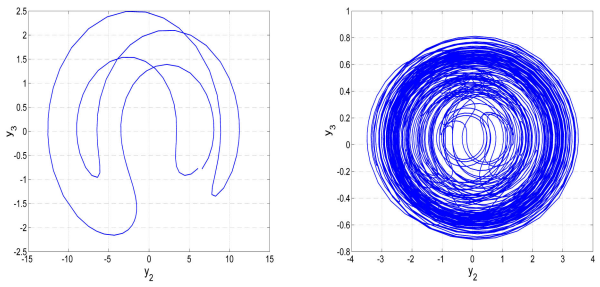

(a) $d = 4.7$ (b) $d = 0.2$

(c) $d = 2$

FIGURE 15. 2-D plots of the new 4-D system (1) in the (y_1, y_4) -plane for $a = 1, b = 0.8$ $c = 20$ and different values of d: (a) periodic attractor ($d = 4.7$), (b) chaotic attractor ($d = 0.2$) and (c) hyperchaotic attractor ($d = 2$).

IV. MULTISTABILITY AND COEXISTING ATTRACTORS IN THE NEW 4-D HYPERCHAOTIC SYSTEM

To investigate the impact of initial conditions on the behaviour of the new 4-D system (1), the bifurcation diagram of system (1) versus parameter a for two different initial conditions is calculated and plotted. The system (1) remains invariant under the transformation of coordinates

$$S : (y_1, y_2, y_3, y_4) \mapsto (-y_1, -y_2, y_3, -y_4) \tag{24}$$

Thus, any projection of the attractor has rotational symmetry in the y_3-axis. Thus, the system (1) may exhibit coexisting attractors. The bifurcation diagram obtained enables us to observe the phenomenon of multistability and the appearance of coexisting attractors.

Let X_1 and X_2 be two different initial conditions for the new 4-D system (1), where:

$$X_1 = (1, 1, 1, 1) \text{ (Blue color)} \tag{25}$$
$$X_2 = (-1, -1, 1, -1) \text{ (Red color)} \tag{26}$$

We fix the values of system parameters as

$$b = 1.5, \quad c = 25, \quad d = 10 \tag{27}$$

It can be observed from the bifurcation diagram shown in Figure 16 that the new 4-D system (1) has two different dynamical evolutions when a varies in the interval [1, 5].

When we set $a = 1.4$, the system (1) shows two coexisting periodic attractors starting from X_1 (blue color) and X_2 (red color) as shown in Figure 17 (a).

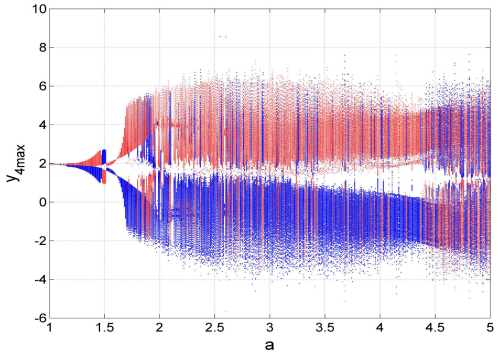

FIGURE 16. The bifurcation diagram of the system (1) with $b = 1.5$, $c = 25$, $d = 10$ and $a \in [1, 5]$: X_1 (blue color) and X_2 (red color).

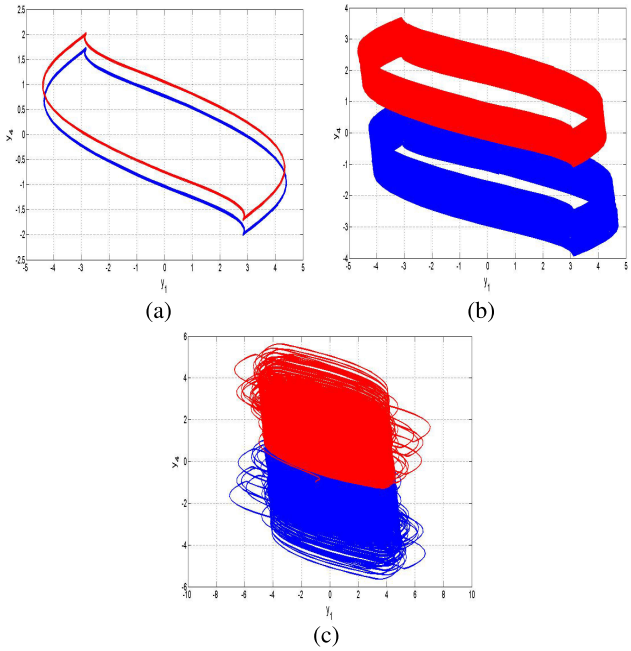

(a) (b)

(c)

FIGURE 17. Matlab phase plots of the various coexisting attractors of the system (1) in the (y_1, y_4)-plane: (a) the coexisting periodic attractors for $a = 1.4$, (b) the coexisting chaotic attractors for $a = 1.75$ and (c) the coexisting hyperchaotic attractors for $a = 3.5$.

When we set $a = 1.75$, the system (1) shows two coexisting chaotic attractors starting from X_1 (blue color) and X_2 (red color) as shown in Figure 17 (b). The two coexisting attractors have the same values of Lyapunov exponents:

$$LE_1 = 0.022, \quad LE_2 = 0,$$
$$LE_3 = -0.622, \quad LE_4 = -1.084 \tag{28}$$

When we set $a = 3.5$, the system (1) shows two coexisting hyperchaotic attractors starting from X_1 (blue color) and X_2 (red color) as shown in Figure 17 (c). The two coexisting attractors have the same values of Lyapunov exponents:

$$LE_1 = 0.135, \quad LE_2 = 0.040,$$
$$LE_3 = 0, \quad LE_4 = -3.665 \tag{29}$$

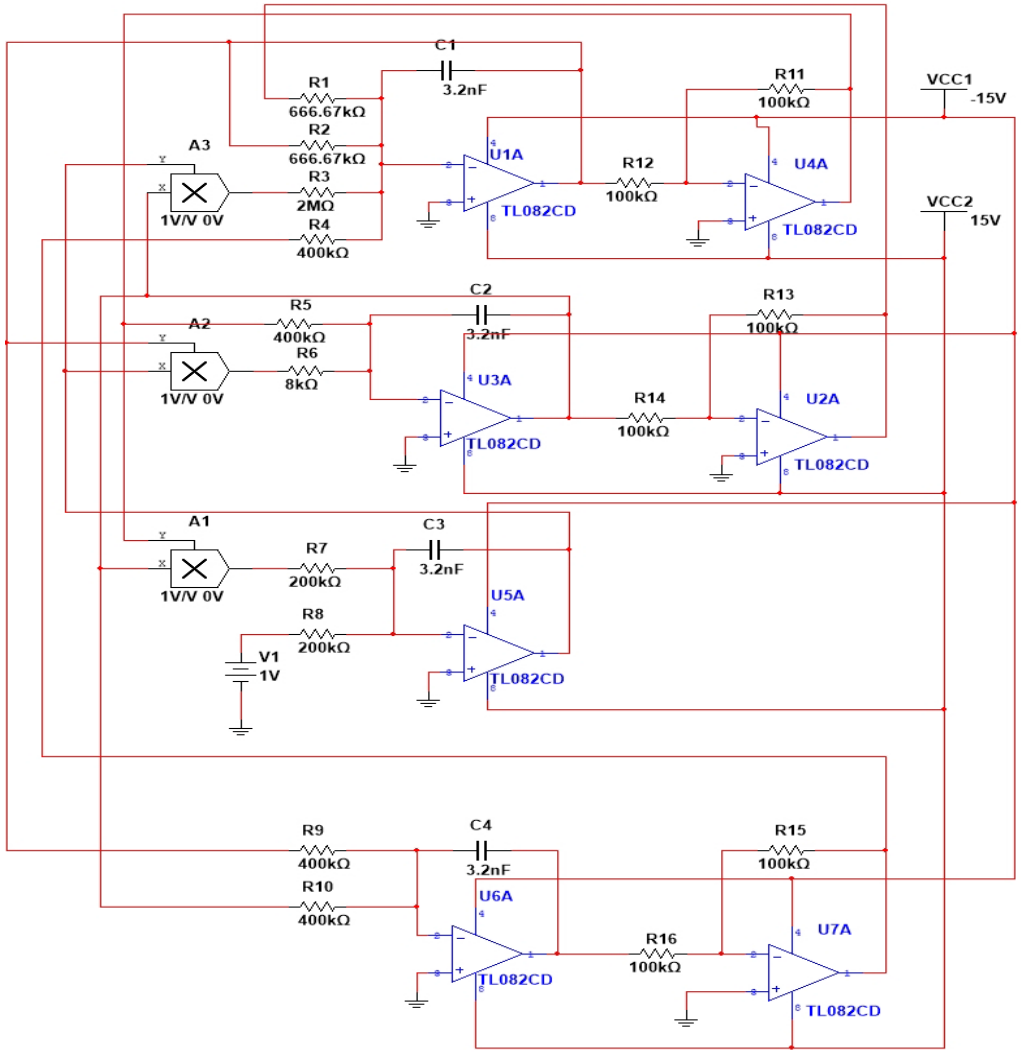

FIGURE 18. Schematic diagram of the electronic circuit of the 4-D hyperchaotic system (32).

V. CIRCUIT DESIGN OF THE NEW HYPERCHAOTIC SYSTEM

In this section, the 4-D hyperchaotic system (1) with no balance point is designed by NI Multisim 14.0 software. The circuit includes 7 operational amplifiers, 3 multipliers, 4 capacitors and 16 resistors. It is noted that the operational amplifiers ($U1A$, $U3A$, $U5A$, $U6A$) are configured as integrators while three operational amplifiers ($U2A$, $U4A$, $U7A$) are configured as inverting amplifier.

For the circuit design, the new 4-D hyperchaotic system (1) has to be rescaled by using

$$Y_1 = \frac{1}{2}y_1, Y_2 = \frac{1}{2}y_2, Y_3 = \frac{1}{2}y_3, \quad Y_4 = \frac{1}{2}y_4 \tag{30}$$

This results in the following 4-D hyperchaotic system in the new coordinates:

$$\begin{cases} \dot{Y}_1 = a(Y_2 - Y_1) - 2bY_2Y_3 + Y_4 \\ \dot{Y}_2 = Y_1 - 2cY_1Y_3 \\ \dot{Y}_3 = 2Y_1Y_2 - 2 \\ \dot{Y}_4 = -Y_1 - Y_2 \end{cases} \tag{31}$$

The circuit equation of the 4-D hyperchaotic system (31) after using Kirchhoff's electrical circuit laws can be derived as follows:

$$\begin{cases} \dot{Y}_1 = \dfrac{1}{C_1R_1}Y_2 - \dfrac{1}{C_1R_2}Y_1 - \dfrac{1}{C_1R_3}Y_2Y_3 \\ \qquad + \dfrac{1}{C_1R_4}Y_4 \\ \dot{Y}_2 = \dfrac{1}{C_2R_5}Y_1 - \dfrac{1}{C_2R_6}Y_1Y_3 \\ \dot{Y}_3 = \dfrac{1}{C_3R_7}Y_1Y_2 - \dfrac{1}{C_3R_8}V_1 \\ \dot{Y}_4 = -\dfrac{1}{C_4R_9}Y_1 - \dfrac{1}{C_4R_{10}}Y_2 \end{cases} \tag{32}$$

Here, Y_1, Y_2, Y_3, Y_4 are the voltages across the capacitors, C_1, C_2, C_3, C_4, respectively. We choose the values of the circuital elements as follows: $R_1 = R_2 = 666.67$ kΩ, $R_3 = 2$ MΩ, $R_4 = R_5 = R_9 = R_{10} = 400$ kΩ, $R_6 = 8$ kΩ, $R_7 = R_8 = 200$ kΩ, $R_{11} = R_{12} = R_{13} = R_{14} = R_{15} = R_{16} = 100$ kΩ and $C_1 = C_2 = C_3 = C_4 = 3.2$ nF.

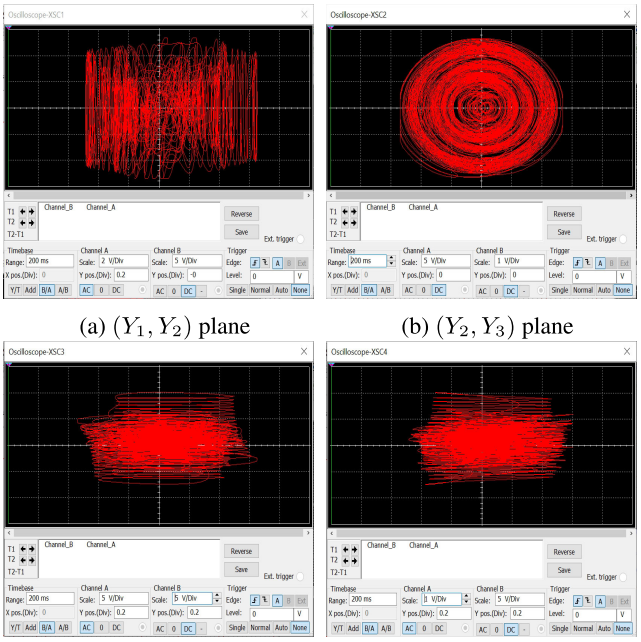

(a) (Y_1, Y_2) plane (b) (Y_2, Y_3) plane

(c) (Y_2, Y_4) plane (d) (Y_3, Y_4) plane

FIGURE 19. 2*D* signal plots of the 4-D hyperchaotic circuit (32) using NI Multisim 14.0 circuit simulation.

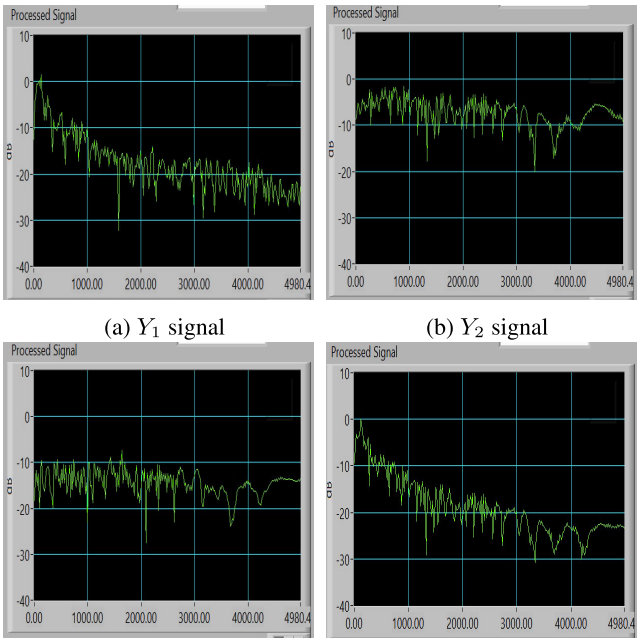

(a) Y_1 signal (b) Y_2 signal

(c) Y_3 signal (d) Y_4 signal

FIGURE 20. Fourier spectral analysis plots of the 4-D hyperchaotic circuit (32) using NI Multisim 14.0 circuit simulation.

The electronic circuit of the new 4-D hyperchaotic system (32) is constructed and shown in Figure 18. The NI Multisim 14.0 phase portraits in Figure 19 verify the hyperchaotic behavior of the 4-D circuit (32).

The Fourier spectral distributions for the variables Y_1, Y_2, Y_3, Y_4 of the circuit (32) are shown in Figure 20. The frequency range is 5 kHz and maximum peak 500 Hz. It corresponds to a prevailing frequency of the implementing oscillating loop. The power spectra of the output signals in Figure 20 are broadband, which are typical of hyperchaotic signals.

VI. FPGA DESIGN OF THE NEW 4-D HYPERCHAOTIC SYSTEM

It is well-known that FPGAs are quite useful for fast prototyping, easy of reprogrammability and reconfigurability, and they provide low development cost applications, while maintaining good performance. However, for solving hyper-chaotic systems, the required hardware resources and processing time depend on the numerical method. In this manner, this section shows the FPGA implementation of the new 4-D hyperchaotic system given in (1) by applying three numerical methods, namely: Forward-Euler, Backward-Euler and fourth-order Runge-Kutta methods. As highlighted in [22], each numerical method provides different accuracy and requires a good estimation of the step-size to diminish numerical errors. For instance, by applying the Forward Euler method, one gets the discrete equations given by (33), from which one can infer the use of multipliers, adders and subtractors for the FPGA implementation.

$$\begin{aligned} y1_{n+1} &= y1_n + h[a(y2_n - y1_n) - by2_n y3_n + y4_n] \\ y2_{n+1} &= y2_n + h[y1_n(1 - cy3_n)] \\ y3_{n+1} &= y3_n + h[y1_n y2_n - d] \\ y4_{n+1} &= y4_n + h[-y1_n - y2_n] \end{aligned} \tag{33}$$

From the discretized equations given in (33), one can design the block description as shown in Figure 21. In this figure, one can appreciate the block called single-constant multiplier (SCM), who implements the multiplication of a state variable by a constant a, b, c, d. This SCM block is designed with adders, subtractors and shift registers in order to reduce hardware resources compared to using a traditional multiplier [20]. The SCM is also designed for all the blocks multiplying the step-size h in the blocks labeled as Predictor Forward-Euler.

The synthesis of all the blocks can be designed by adopting fixed-point representation with the format 13.19 (32 bits), using one bit for the sign, 12 for the integer part, and 19 for the fractional part. It is worth mentioning that this 13.19 format is established by the computer arithmetic and depends on the amplitudes of the state variables. For example, simulation results for this new 4-D hyperchaotic system (1) provide the ranges $[-10, 13]$ for y_1, $[-28, 28]$ for y_2, $[-8, 8]$ for y_3 and $[-15, 20]$ for y_4, but in the discretization of the second equation, the expected result of $y1_n(1 - cy3_n)$ is ± 2500, and therefore, this value can be represented by using 12 bits in the integer part.

The block description of the new 4-D hyper-chaotic system (1) by applying Backward-Euler method, is shown

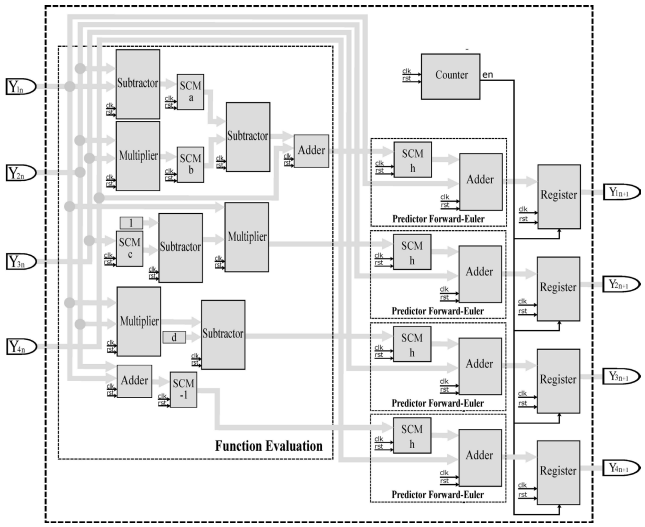

FIGURE 21. Block diagram of the new 4-D hyperchaotic system given in (1) discretized with the Forward Euler method.

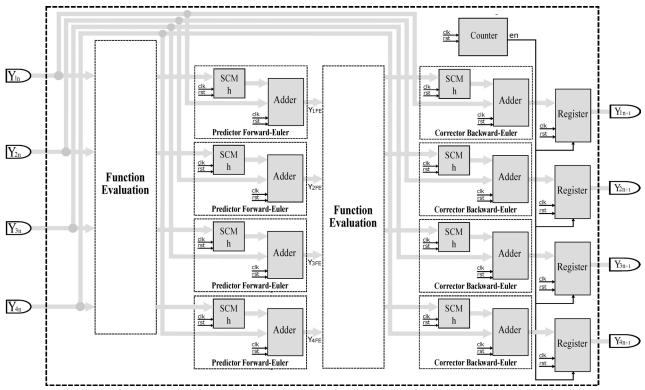

FIGURE 22. Block diagram of the new 4-D hyperchaotic system (1) discretized with the Backward Euler method.

in Figure 21. It can be appreciated that this description embeds the Forward Euler method in the blocks labeled as Predictor Forward Euler, and it does a correction by the blocks labeled Corrector Backward Euler. Again, the hardware resources are reduced for FPGA implementation by using SCMs, adders and registers. The application of the fourth-order Runge-Kutta method is performed in the same way, as detailed in [20].

In this work, we set $h = 0.01$, and Table 2 shows the resources of the implementation of (1) by using the FPGA Cyclone IV EP4CGX150DF31C7 along the synthesizer "Quartus II 13.0". It is worthy mentioning that the row called "Clock cycles by iteration" represents the number of clock cycles that are required to process a new iteration to compute $y1_{n+1}, y2_{n+1}, y3_{n+1}$ and $y4_{n+1}$ with a valid data, and the "Latency" row represents the time to compute a new iteration with a 50 MHz clock signal.

Figure 23 shows the experimental setup to implement the new 4-D hyperchaotic system (1) in the FPGA Cyclone IV EP4CGX150DF31C7. A 16-bit Digital-to-Analog converter

TABLE 2. Hardware resources for the implementation of the 4-D hyperchaotic system (1) by using the FPGA cyclone IV EP4CGX150DF31C7, and by applying the Forward Euler, Backward Euler and fourth order Runge-Kutta methods with $h = 0.01$.

Resources	Forward Euler	Backward Euler	4th order Runge Kutta	Available
Logic Elements	1375	3116	6774	149,760
Registers	777	1825	3289	149,760
9×9 Bit multipliers	48	96	128	720
Max Freq. (MHz)	97.96	88.04	89.88	50
Clock cycles by Iteration	10	18	36	-
Latency (ns)	200	360	720	-

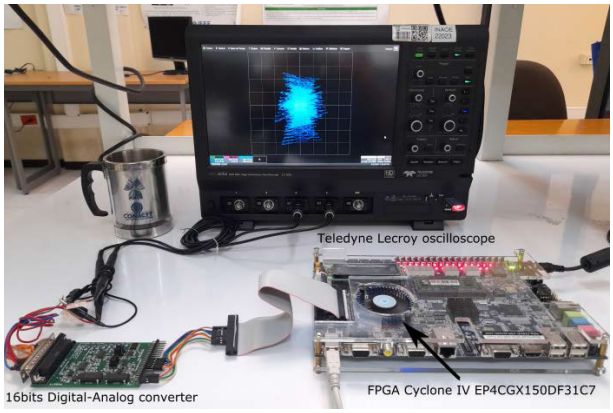

FIGURE 23. Experimental setup to implement the 4-D hyperchaotic system (1) using a FPGA Cyclone IV EP4CGX150DF31C7, a 16-bit Digital-Analog converter and a Teledyne Lecroy oscilloscope to visualize the attractor.

is used to visualize the results in the Teledyne Lecroy oscilloscope. Figure 24 shows the experimental time series of the state variables of (1) applying Forward Euler method. Figures 25, 26, and 27, show the experimental hyperchaotic attractors of FPGA implementation of (1)by applying the Forward Euler, Backward Euler and the fourth-order Runge Kutta methods.

VII. IMAGE CRYPTOSYSTEM BASED ON THE NEW 4-D HYPERCHAOTIC SYSTEM

In this section, we design a novel image encryption algorithm using the nonlinear features of the proposed 4-D hyperchaotic system (1). To accommodate the hyperchaotic system (1) for the aims of designing modern cryptographic purposes such as high security and low computational power, the proposed hyperchaotic system (1) is adapted to be iterative as presented in Eq. (34).

$$\begin{cases} y1_{t+1} = (a\,(y2_t - y1_t) - b\,y2_t y3_t + y4_t)\,mod\,1 \\ y2_{t+1} = (y1_t(1 - cy3_t))\,mod\,1 \\ y3_{t+1} = (y1_t y2_t - d)\,mod\,1 \\ y4_{t+1} = (-y1_t - y2_t)\,mod\,1 \end{cases} \tag{34}$$

A. ENCRYPTION ALGORITHM

The proposed image cryptosystem utilizes the hash code for the pristine image to update the primary conditions of the

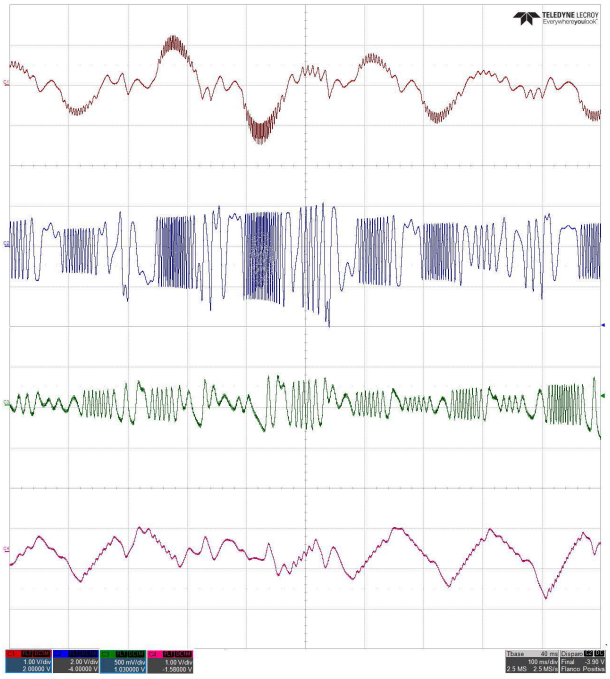

FIGURE 24. Experimental time series of the 4-D hyperchaotic system (1) observed by applying the Forward Euler method with step-size $h = 1 \times 10^{-5}$.

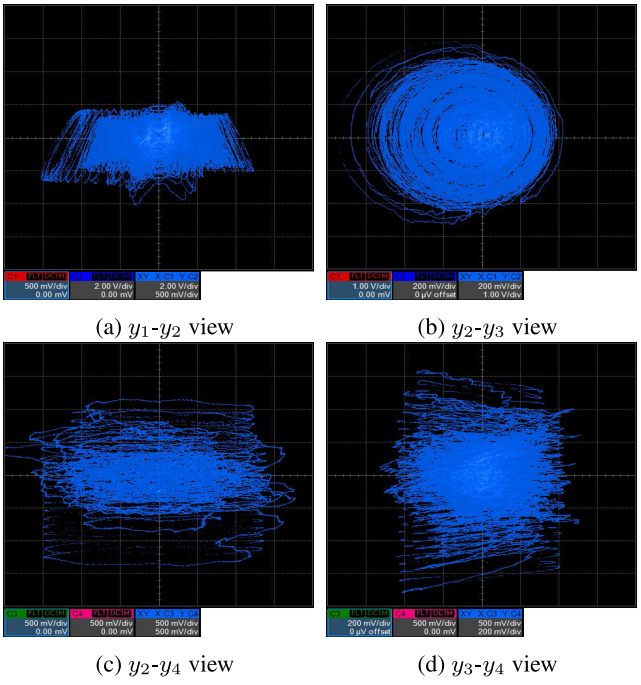

FIGURE 25. Hyperchaotic attractors of the 4-D system (1) from the FPGA implementation by applying the Forward Euler method with step-size $h = 1 \times 10^{-5}$. (a) y_1-y_2 view, (b) y_2-y_3 view, (c) y_2-y_4 view and (d) y_3-y_4 view).

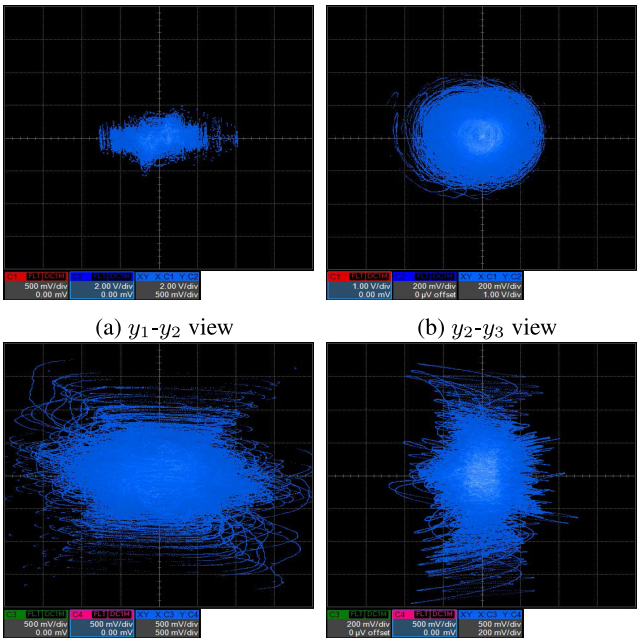

FIGURE 26. Hyperchaotic attractors of the 4-D system (1) from the FPGA implementation by applying the Backward Euler method with step-size $h = 1 \times 10^{-3}$. (a) y_1-y_2 view, (b) y_2-y_3 view, (c) y_2-y_4 view and (d) y_3-y_4 view).

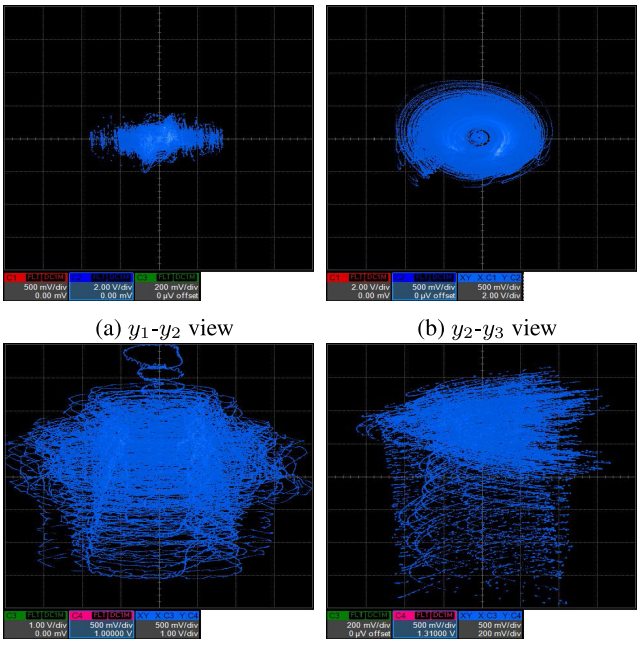

FIGURE 27. Hyperchaotic attractors of the 4-D system (1) from the FPGA implementation by applying the fourth order Runge Kutta method with step-size $h = 1 \times 10^{-3}$. (a) y_1-y_2 view, (b) y_2-y_3 view, (c) y_2-y_4 view and (d) y_3-y_4 view).

hyperchaotic system. The outcome of iterating the hyperchaotic system is four chaotic sequences ($Y1$, $Y2$, $Y3$, and $Y4$), the last chaotic sequence ($Y4$) is utilized for constructing a new chaotic sequence (Q) from the other sequences ($Y1$, $Y2$, and $Y3$), and the pristine image is permutated then substituted utilizing sequence Q. The proposed encryption mechanism is described in Figure 28, while the steps of the encryption procedure are described in Algorithm 1.

Algorithm 1 Encryption Procedure

Input: Pristine image (*PrImg*)

Parameter: Initial conditions and control parameters for iterating the hyperchaotic system ($y1_{initial}$, $y2_{initial}$, $y3_{initial}$, $y4_{initial}$, a, b, c, d)

Output: Cipher-image (*CrImg*), some information about the hash value ($H1, H2, H3, H4$)

$Hash \leftarrow SHA256(PrImg)$ // Acquire the hash value for the pristine image

$h \leftarrow uint8(Hash)$ // Convert each 8-bit into an integer number

$H1 \leftarrow (h_1 \oplus h_2 \oplus \cdots \oplus h_8)/256$

$H2 \leftarrow (h_9 \oplus h_{10} \oplus \cdots \oplus h_{16})/256$

$H3 \leftarrow (h_{17} \oplus h_{18} \oplus \cdots \oplus h_{24})/256$

$H4 \leftarrow (h_{25} \oplus h_{26} \oplus \cdots \oplus h_{32})/256$

// Update initial conditions ($y1_{initial}$, $y2_{initial}$, $y3_{initial}$, $y4_{initial}$)

$y1_{new} \leftarrow (y1_{initial} + H1)/2$

$y2_{new} \leftarrow (y2_{initial} + H2)/2$

$y3_{new} \leftarrow (y3_{initial} + H3)/2$

$y4_{new} \leftarrow (y4_{initial} + H4)/2$

$[Rows \ \ Columns \ \ Depth] \leftarrow size(PrImg)$ // Acquire the dimension of the pristine image

$[Y1 \ \ Y2 \ \ Y3 \ \ Y4] \leftarrow System(y1_{new}, y2_{new}, y3_{new}, y4_{new}, a, b, c, d, Rows \times Columns \times Depth)$ // Iterating the hyperchaotic system (34) for $Rows \times Columns \times Depth$ times

$P_t \leftarrow round(Y4_t \times 10^4) \mod 3 \quad for \quad t \leftarrow 1, 2, \ldots, Rows \times Columns \times Depth$

$$Q_t \leftarrow \begin{cases} Y1_t \ if \ P_t = 0 \\ Y2_t \ if \ P_t = 1 \\ Y3_t \ if \ P_t = 2 \end{cases} \quad for \quad t \leftarrow 1, 2, \ldots, Rows \times Columns \times Depth$$

// Permutation process

$A \leftarrow arrange(Q)$ // Arrange the ingredients of Q in ascending order

$V \leftarrow index(Q, A)$// Take the index of every element of Q in A

$ImgVec \leftarrow reshape(PrImg, Rows \times Columns \times Depth, 1)$ // Convert the pristine image to a one vector

$ImgPer(t) \leftarrow ImgVec(V(t)) \quad for \quad t \leftarrow 1, 2, \ldots, Rows \times Columns \times Depth$

// Substitution process

$Key \leftarrow round(Q \times 10^{14}) \mod 256$ // Transforming Q sequence into integers

$CrImgVec \leftarrow ImgPer \oplus key$// Pixel substitution

$CrImg \leftarrow reshape(CrImVec, Rows, Columns, Depth)$ // Cipher image

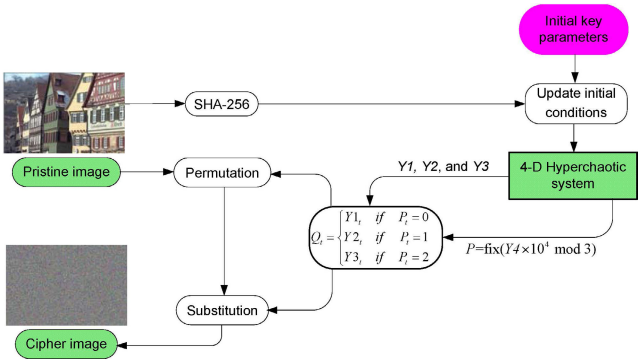

FIGURE 28. Representation of the encryption procedure for the suggested image cryptosystem.

B. EXPERIMENTAL OUTCOMES

To prove the cryptographic characteristics of the proposed image encryption algorithm, a PC with Intel^{R} Core^{TM} 2 Duo CPU 3GHz and RAM 4GB and prepared with MATLAB software R2016b. The used dataset of images was token from Kodak database [34] each of size 768 × 512 and labeled as *PrImg*01, *PrImg*02, *PrImg*03, and *PrImg*04 (see Figure 29). The primary key parameters employed for iterating the hyperchaotic system (34) are fixed as ($y1_{initial} \leftarrow 0.6$, $y2_{initial} \leftarrow 0.8$, $y3_{initial} \leftarrow 0.6$, $y4_{initial} \leftarrow 0.8$, $a \leftarrow 0.6$, $b \leftarrow 0.1$, $c \leftarrow 25$, $d \leftarrow 4$).

1) CORRELATION ANALYSIS

To evaluation the meaningful of an image, the correlation coefficient of neighboring pixels (C_{pc}) is utilized, in which pristine images have C_{pc} values nearby to 1 per direction while the values of C_{pc} for cipher images should around 0 [25]. To compute the values of C_{pc} in each direction of the pristine and cipher images, we randomly picked 10^4 pairs of adjoining pixels per direction.

$$C_{pc} = \frac{\sum_{i=1}^{N} (p_i - \bar{p})(c_i - \bar{c})}{\sqrt{\sum_{i=1}^{N} (p_i - \bar{p})^2 \sum_{i=1}^{N} (c_i - \bar{c})^2}} \tag{35}$$

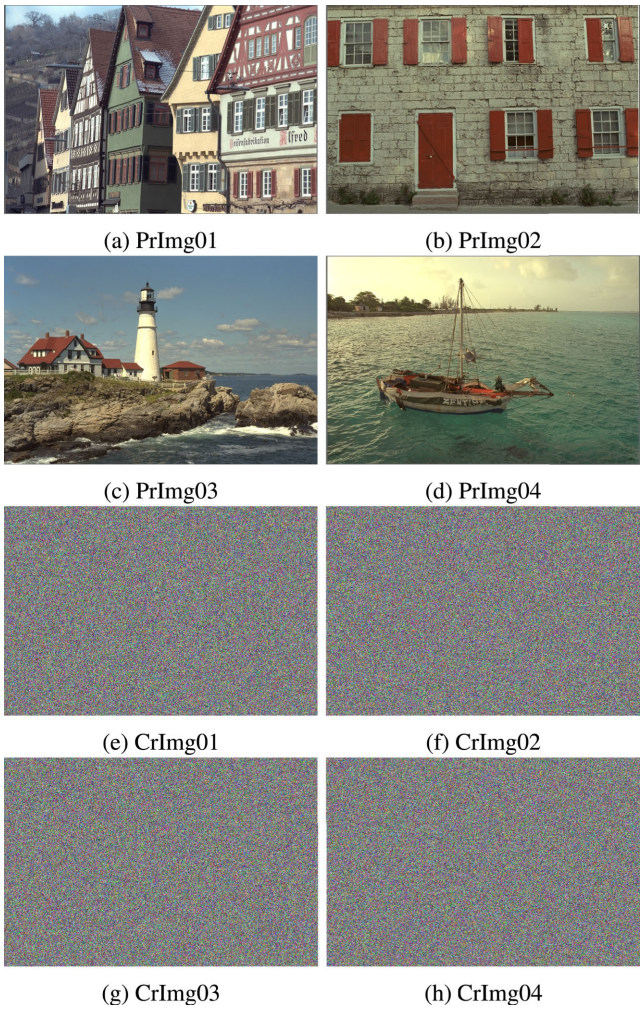

FIGURE 29. Experimental dataset of images and their ciphered ones.

here N refers to the full number of neighboring pixel pairs per direction and c_i, p_i are point to the values of neighboring pixels. Table 3 displays the outputs of C_{pc} for pristine images and their analog cipher version, in which the values of encrypted images are very near to 0. Also, Figs. 30, 31, and 32 plot the correlation distribution per direction for pristine image *PrImg*01 and its analogue cipher version. From the results listed about correlation coefficients, no valuable data acquired about the pristine image by analyzing C_{pc} values.

2) PRISTINE IMAGE SENSITIVITY

To evaluate the outcome of slight modification in the pristine image on its analog cipher version, two measures are employed: "Number of Pixels Change Rate" (NPCR) and "Unified Average Changing Intensity" (UACI). NPCR and UACI can be expressed mathematically as follows:

$$NPCR = \frac{\sum_{i,j} Diff(i,j)}{N} \times 100\%,$$
$$Diff(i,j) = \begin{cases} 0 \ if \ \ Cp1(i,j) = Cp2(i,j) \\ 1 \ if \ \ Cp1(i,j) \neq Cp2(i,j) \end{cases} \quad (36)$$

TABLE 3. C_{pc} values of adjacent pixels for the investigated dataset.

Image	Component	Direction		
		H	V	D
PrImg01	Red	0.9260	0.8830	0.8186
	Green	0.9248	0.8907	0.8245
	Blue	0.9055	0.8612	0.7776
CrImg01	Red	0.0009	0.0001	0.0005
	Green	0.0006	-0.0005	-0.0001
	Blue	-0.0009	-0.0008	-0.0003
PrImg02	Red	0.7877	0.8538	0.7078
	Green	0.8702	0.8995	0.8134
	Blue	0.8448	0.8875	0.7815
CrImg02	Red	0.0013	-0.0008	-0.0006
	Green	0.0005	0.0004	-0.0009
	Blue	0.0002	-0.0001	0.0001
PrImg03	Red	0.8956	0.9401	0.8586
	Green	0.9139	0.9515	0.8831
	Blue	0.9272	0.9587	0.9064
CrImg03	Red	-0.0005	-0.0001	0.0012
	Green	0.0004	0.0002	0.0014
	Blue	0.0003	0.0002	0.0001
PrImg04	Red	0.9480	0.9802	0.9376
	Green	0.9370	0.9718	0.9202
	Blue	0.9147	0.9654	0.8959
CrImg04	Red	-0.0005	0.0006	0.0001
	Green	0.0004	0.0011	-0.0003
	Blue	-0.0006	-0.0005	0.0002

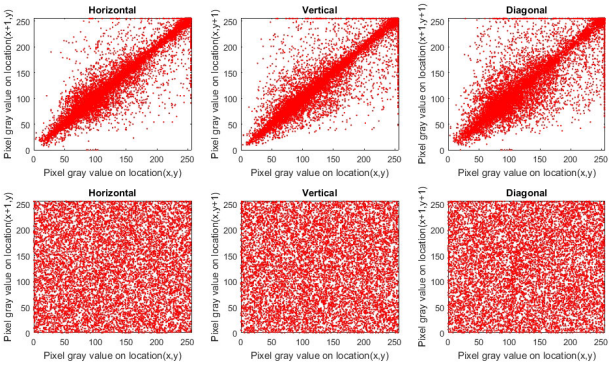

FIGURE 30. Correlation distributions for red component of PrImg01 image, in which the top row provides the distribution for pristine image PrImg01 while the second row indicates the distribution for ciphered image CrImg01.

$$UACI = \frac{1}{N}\left(\sum_{i,j} \frac{|Cp1(i,j) - Cp2(i,j)|}{256}\right) \times 100\% \quad (37)$$

where N refers to the total number of pixels that represent the image and $Cp1$, $Cp2$ are two ciphered images for one pristine image with a difference in one bit. NPCR and UACI values are listed in Table 4, in which the average value of NPCR for the investigated dataset is 99.6125%, therefore the presented image cryptosystem has a high sensitivity for small pixel changes in the pristine image.

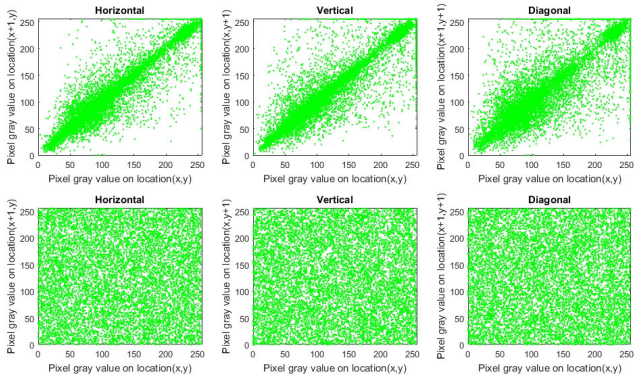

FIGURE 31. Correlation distributions for green component of PrImg01 image, in which the top row provides the distribution for pristine image PrImg01 while the second row indicates the distribution for ciphered image CrImg01.

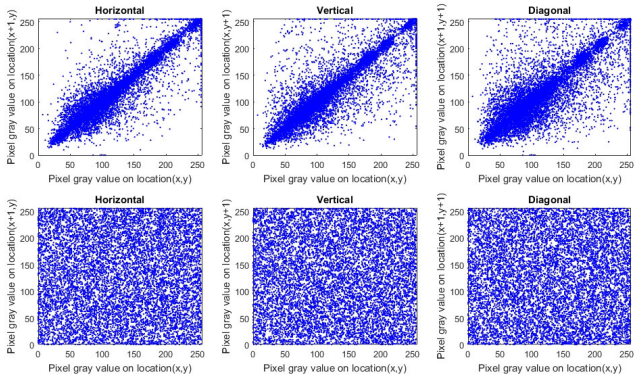

FIGURE 32. Correlation distributions for blue component of PrImg01 image, in which the top row provides the distribution for pristine image PrImg01 while the second row indicates the distribution for ciphered image CrImg01.

TABLE 4. Values of NPCR and UACI for investigated images.

Image	NPCR	UACI
PrImg01	99.6129 %	33.4716 %
PrImg02	99.6101 %	33.4965 %
PrImg03	99.6140 %	33.4588 %
PrImg04	99.6128 %	33.4945 %

3) HISTOGRAM ANALYSIS

To provide the distribution rate of pixel values in an image, histogram test is utilized. The histogram of encrypted images utilizing a good-designed image encryption approach should ensure the identical distribution of different encrypted images to resist statistical attacks [35]. Fig. 33 presents the histograms of image *PrImg*01 before and after the encryption procedure, in which the histograms of the pristine image are distinct from each other while the histograms of the ciphered image *CrImg*01 are uniform with each other. Nevertheless, we need a quantitative tool to measure the pixel distribution in an image. Consequently, we utilized chi-square

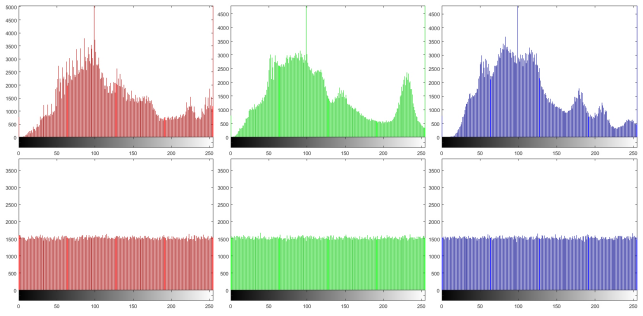

FIGURE 33. Histograms of image PrImg01, in which the first row describes the histograms of pristine image PrImg01 and the last row denotes the histograms of ciphered image CrImg01.

TABLE 5. χ^2 values of the investigated images.

Image	χ^2 value		
	Red	Green	Blue
PrImg01	285277.4635	219680.6289	221228.6081
PrImg02	517987.2604	343407.2395	406802.7187
PrImg03	547600.2122	631414.9388	1080010.4479
PrImg04	739392.7942	670065.1757	288739.7005
CrImg01	276.9076	258.0456	256.2422
CrImg02	279.1680	238.8919	277.7682
CrImg03	271.7122	264.0352	248.2461
CrImg04	242.8750	218.2057	221.0794

TABLE 6. Information entropy for the investigated dataset.

Image	Pristine	Cipher
PrImg01	7.673795	7.999827
PrImg02	7.326479	7.999831
PrImg03	7.259478	7.999841
PrImg04	7.520453	7.999863

test (χ^2) [27].

$$\chi^2 = \sum_{t=0}^{255} \frac{(f_t - d)^2}{d} \tag{38}$$

where f_t refers to the frequency of pixel value t, and d indicates the size of the image. By considering the significant level is 0.05, then $\chi^2_{0.05}(255) = 293.25$. For a given image, if the value of χ^2 is less than 293.25, this points that the given image has an identical distribution; else, the image holds non-identical distribution. Table 5 provides the outcome of χ^2 for the examined images, in which the χ^2 values for all encrypted images is less than 293.25. Therefore, the provided encryption mechanism can withstand histogram analysis attacks.

4) INFORMATION ENTROPY ANALYSIS

To provide the distribution of pixel values per level in an image, information entropy test is utilized and can be stated

TABLE 7. Encryption time (in s) for the stated cryptosystem alongside other related cryptosystems for different dimensions of images.

Cryptosystem	Image dimension		
	256×256	512×512	1024×1024
Proposed	0.0499	0.2576	0.9762
[38]	0.0538	0.2338	1.1494
[39]	0.0949	0.4010	1.9857
[40]	0.1789	0.6639	3.1426
[41]	0.0779	0.3261	1.3146
[35]	0.0494	0.3034	1.0454

mathematically as given in Eq. (39):

$$E(X) = -\sum_{t=0}^{255} p(x_t) \log_2 (p(x_t)) \tag{39}$$

where $p(x_t)$ refers the probability of x_t. The possible values for a grayscale image are 2^8, so the optimal entropy value is equal to 8-bit [36], [37]. Subsequently, to approve the effectiveness of the proposed encryption algorithm, the entropy value of the ciphered images should be close to 8. Table 6 provides the outcome of the entropy test for the pristine images and their analogous encrypted version, in which all information entropy values for encrypted images are very nearby to 8-bit. Consequently, the suggested encryption algorithm is secure against entropy attacks.

5) KEY SENSITIVITY ANALYSIS

The sensitivity of the secret key to the decryption effect is known as the key sensitivity. To value the key sensitivity of the proposed cryptosystem, the ciphered image *CrImg*01 decrypted several times with slight modification in the secret key each time, in which the results are stated in Fig. 34.

6) OCCLUSION ATTACKS

Data may suffer from losing some of its parts when transmitted over a noisy channel [30]. Hence, the proposed image cryptosystem must have the capability to resist occlusion attacks. To value the proposed encryption approach against these attacks, we clipping out some parts of the encrypted image and then trying to decrypt the defective cipher image.

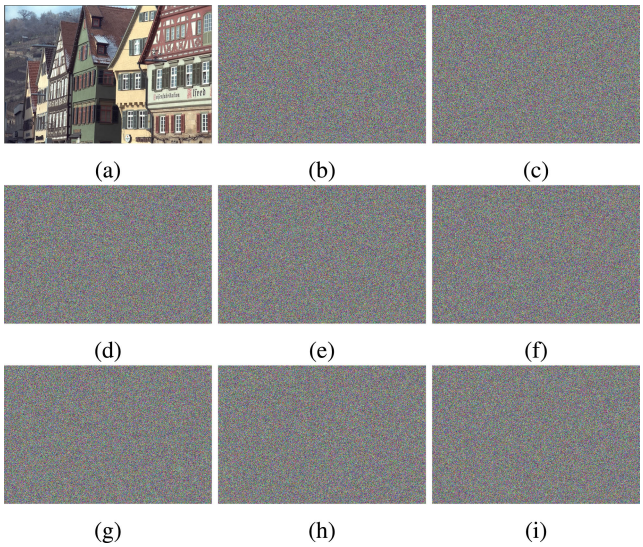

FIGURE 34. Decryption process for the ciphered image *CrImg*01 several times with slight modification in the secret key each time: (a) True key, (b) True key except for $y1_{initial} = 0.6 + 10^{-16}$, (c) True key except for $y2_{initial} = 0.8 + 10^{-16}$, (d) True key except for $y3_{initial} = 0.6 + 10^{-16}$, (e) True key except for $y4_{initial} = 0.8 + 10^{-16}$, (f) True key except for $a = 0.6 + 10^{-16}$, (g) True key except for $b = 0.1 + 10^{-16}$, (h) True key except for $c = 25 + 10^{-14}$ and (i) True key except for $d = 4 + 10^{-15}$.

Figure 35 provides results of occlusion attacks, in which the pristine image is recovered effectively from the defective cipher image without information losing in the clipped part.

7) TIME EFFICIENCY AND COMPARISON ANALYSIS

The main contribution of designing modern cryptographic mechanisms is to provide high security in addition to low computational power. To confirm that the suggested image cryptosystem is efficient in time encryption, we calculate the time required to encrypt one image. Table 7 provides the time taken to encrypt several grayscale images with diverse dimensions alongside other related cryptosystems, in which the proposed image cryptosystem is effective in time encryption. To confirm that the suggested image cryptosystem has high security compared to other related cryptosystems, Table 8 gives a simple comparison in terms of average values of correlation, information entropy, NPCR, UACI, and Chi-square.

TABLE 8. Comparison of the proposed encryption mechanism with other related mechanisms in terms of average values of correlation, information entropy, UACI, NPCR, and Chi-square.

Cryptosystem	Correlation			Information entropy	χ^2	NPCR	UACI
	H	V	D				
Proposed	0.00018	-0.00002	0.00012	7.99984	254.4314	99.613%	33.483%
[42]	0.00050	0.00170	-0.00250	7.99866	256.7515	99.607%	33.427%
[43]	-0.00063	0.00083	-0.00034	7.99930	264.4174	99.600%	33.473%
[44]	-0.00970	-0.00870	0.00650	7.99700	257.3367	99.600%	33.440%
[45]	0.00219	0.00169	0.00186	7.99929	249.4286	99.611%	33.476%
[35]	-0.00016	0.00002	0.00023	7.99949	250.5122	99.622%	33.472%
[46]	0.00007	0.00007	-0.00014	7.99984	-	99.608%	33.470%
[36]	0.00267	-0.00008	-0.00007	7.99720	254.9902	99.633%	33.530%
[27]	0.00020	-0.00010	-0.00010	7.99976	256.3767	99.606%	-
[28]	-0.00028	0.00016	0.00018	7.99984	257.3172	99.604%	33.459%

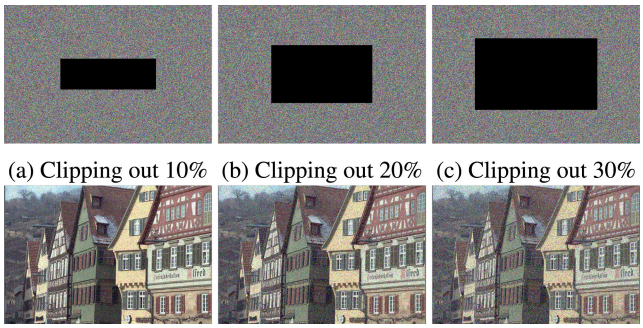

(a) Clipping out 10% (b) Clipping out 20% (c) Clipping out 30%

FIGURE 35. Results of occlusion attack, in which the first row expresses the defective ciphered images and the last row express the corresponding recovered ones.

From the stated values in Tables 7 and 8, we declare that the presented image cryptosystem is effective and has high security besides low encryption time.

VIII. CONCLUSION

This work started with a dynamical model of a new 4-D hyperchaotic system with no balance point and presented a detailed bifurcation analysis for the new hyperchaotic dynamo system with respect to the system parameters. We noted that the new hyperchaotic system displays multistability with coexisting attractors. Using NI Multisim 14.0 software, we designed an electronic circuit for the implementation of the new 4-D hyperchaotic system and presented the circuit simulation results. We also detailed the implementation of the new 4-D hyperchaotic system by using a field programmable gate array (FPGA). The FPGA design was done by applying three numerical methods, namely: Forward-Euler, Backward-Euler and fourth-order Runge-Kutta methods. We demonstrate that experimental chaotic attractors were in good agreement with the Matlab simulations. In addition, this work presented a new image cryptosystem using the nonlinearity features of the new 4-D hyperchaotic system with no balance point, which the simulation outcomes confirm the effectiveness of the proposed cryptosystem and the reliability of the hyperchaotic system in designing various modern cryptographic applications.

REFERENCES

[1] C. Bonatto, "Hyperchaotic dynamics for light polarization in a laser diode," *Phys. Rev. Lett.*, vol. 120, no. 16, Apr. 2018, Art. no. 163902.

[2] E. Barakat, M. Abdel-Aty, and I. L. El-Kalla, "Hyperchaotic and quasiperiodic behaviors of a two-photon laser with multi-intermediate states," *Chaos, Solitons Fractals*, vol. 152, Nov. 2021, Art. no. 111316.

[3] E. Petavratzis, C. Volos, H. Nistazakis, I. Stouboulos, and I. Kyprianidis, "An improved motion controller of a mobile robot based on a hyperchaotic system," *Int. J. Mech.*, vol. 12, pp. 200–204, 2018.

[4] S. Vaidyanathan, I. Moroz, and A. Sambas, "A new hyperjerk dynamical system with hyperchaotic attractor and two saddle-focus rest points exhibiting Hopf bifurcations, its hyperchaos synchronisation and circuit implementation," *Int. J. Model., Identificat. Control*, vol. 33, no. 4, pp. 299–310, 2019.

[5] J. Luo, S. Qu, Y. Chen, X. Chen, and Z. Xiong, "Synchronization, circuit and secure communication implementation of a memristor-based hyperchaotic system using single input controller," *Chin. J. Phys.*, vol. 71, pp. 403–417, Jun. 2021.

[6] Y. Zhang, L. Zhang, Z. Zhong, L. Yu, M. Shan, and Y. Zhao, "Hyperchaotic image encryption using phase-truncated fractional Fourier transform and DNA-level operation," *Opt. Lasers Eng.*, vol. 143, Aug. 2021, Art. no. 106626.

[7] Y. Bian and W. Yu, "A secure communication method based on 6-D hyperchaos and circuit implementation," *Telecommun. Syst.*, vol. 77, no. 4, pp. 731–751, Aug. 2021.

[8] V. O. Munyaev, D. S. Khorkin, M. I. Bolotov, L. A. Smirnov, and G. V. Osipov, "Appearance of chaos and hyperchaos in evolving pendulum network," *Chaos, Interdiscipl. J. Nonlinear Sci.*, vol. 31, no. 6, Jun. 2021, Art. no. 063106.

[9] H. Ming, H. Hu, and J. Zheng, "Analysis of a new coupled hyperchaotic model and its topological types," *Nonlinear Dyn.*, vol. 105, no. 2, pp. 1937–1952, Jul. 2021.

[10] J. Ying, Y. Liang, G. Wang, H. H.-C. Iu, J. Zhang, and P. Jin, "Locally active memristor based oscillators: The dynamic route from period to chaos and hyperchaos," *Chaos, Interdiscipl. J. Nonlinear Sci.*, vol. 31, no. 6, Jun. 2021, Art. no. 063114.

[11] N. V. Stankevich, A. P. Kuznetsov, and E. P. Seleznev, "Chaos and hyperchaos arising from the destruction of multifrequency tori," *Chaos, Solitons Fractals*, vol. 147, Jun. 2021, Art. no. 110998.

[12] S. Vaidyanathan, S. He, and A. Sambas, "A new multistable double-scroll 4-D hyperchaotic system with no equilibrium point, its bifurcation analysis, synchronization and circuit design," *Arch. Control Sci.*, vol. 31, no. 1, pp. 99–128, 2021.

[13] A. Karthikeyan, S. Çiçek, K. Rajagopal, P. Duraisamy, and A. Srinivasan, "New hyperchaotic system with single nonlinearity, its electronic circuit andencryption design based on current conveyor," *TURKISH J. Electr. Eng. Comput. Sci.*, pp. 1692–1705, May 2021.

[14] S. Vaidyanathan, E. Tlelo-Cuautle, A. Sambas, L. Dolvis, and O. Guillén-Fernández, "FPGA design and circuit implementation of a new four-dimensional multistable hyperchaotic system with coexisting attractors," *Int. J. Comput. Appl. Technol.*, vol. 64, no. 3, pp. 223–234, 2020.

[15] A. Buscarino, L. Fortuna, M. Frasca, and G. Sciuto, *A Concise Guide to Chaotic Electronic Circuits*. Berlin, Germany: Springer, 2014.

[16] A. Sambas, S. Vaidyanathan, I. Moroz, B. Idowu, M. Mohamed, M. Mamat, and W. Sanjaya, "A simple multi-stable chaotic jerk system with two saddle-foci equilibrium points: Analysis, synchronization via backstepping technique and MultiSim circuit design," *Int. J. Electr. Comput. Eng.*, vol. 11, no. 4, pp. 2941–2952, 2021.

[17] B. Idowu, K. Oyeleke, O. Olusola, S. Vaidyanathan, A. Sambas, M. Mohamed, M. Mamat, and Sukono, "Adaptive control and circuit implementation of a new 3-dimensional chaotic system with quadratic, cubic and quartic nonlinearities," *J. Adv. Res. Dyn. Control Syst.*, vol. 12, no. 6, pp. 792–806, 2020.

[18] S. Mobayen, A. Fekih, S. Vaidyanathan, and A. Sambas, "Chameleon chaotic systems with quadratic nonlinearities: An adaptive finite-time sliding mode control approach and circuit simulation," *IEEE Access*, vol. 9, pp. 64558–64573, 2021.

[19] J. Petrzela, "Hyperchaotic self-oscillations of two-stage class C amplifier with generalized transistors," *IEEE Access*, vol. 9, pp. 62182–62194, 2021.

[20] E. Tlelo-Cuautle, J. J. Rangel-Magdaleno, A. D. Pano-Azucena, P. J. Obeso-Rodelo, and J. C. Nunez-Perez, "FPGA realization of multi-scroll chaotic oscillators," *Commun. Nonlinear Sci. Numer. Simul.*, vol. 27, nos. 1–3, pp. 66–80, Oct. 2015.

[21] E. Tlelo-Cuautle, L. G. D. L. Fraga, O. Guillén-Fernández, and A. Silva-Juárez, *Optimization of Integer/Fractional Order Chaotic Systems by Metaheuristics and Their Electronic Realization*. Boca Raton, FL, USA: CRC Press, 2021.

[22] E. Tlelo-Cuautle, A. D. Pano-Azucena, O. Guillén-Fernández, and A. Silva-Juárez, *Analog/Digital Implementation of Fractional Order Chaotic Circuits and Applications*. Berlin, Germany: Springer, 2020.

[23] A. A. A. El-Latif, B. Abd-El-Atty, I. Mehmood, K. Muhammad, S. E. Venegas-Andraca, and J. Peng, "Quantum-inspired blockchain-based cybersecurity: Securing smart edge utilities in IoT-based smart cities," *Inf. Process. Manage.*, vol. 58, no. 4, Jul. 2021, Art. no. 102549.

[24] A. A. A. El-Latif, B. Abd-El-Atty, S. E. Venegas-Andraca, H. Elwahsh, M. J. Piran, A. K. Bashir, O.-Y. Song, and W. Mazurczyk, "Providing end-to-end security using quantum walks in IoT networks," *IEEE Access*, vol. 8, pp. 92687–92696, 2020.

[25] B. Abd-El-Atty, A. M. Iliyasu, A. Alanezi, and A. A. A. El-latif, "Optical image encryption based on quantum walks," *Opt. Lasers Eng.*, vol. 138, Mar. 2021, Art. no. 106403.
[26] A. A. A. El-Latif, B. Abd-El-Atty, M. Amin, and A. M. Iliyasu, "Quantum-inspired cascaded discrete-time quantum walks with induced chaotic dynamics and cryptographic applications," *Sci. Rep.*, vol. 10, no. 1, pp. 1–16, Feb. 2020.
[27] A. Sambas, S. Vaidyanathan, E. Tlelo-Cuautle, B. Abd-El-Atty, A. A. A. El-Latif, O. Guille-Fernandez, Sukono, Y. Hidayat, and G. Gundara, "A 3-D multi-stable system with a peanut-shaped equilibrium curve: Circuit design, FPGA realization, and an application to image encryption," *IEEE Access*, vol. 8, pp. 137116–137132, 2020.
[28] S. Vaidyanathan, A. Sambas, B. Abd-El-Atty, A. A. A. El-Latif, E. Tlelo-Cuautle, O. Guillen-Fernandez, M. Mamat, M. A. Mohamed, M. Alcin, M. Tuna, I. Pehlivan, I. Koyuncu, and M. A. H. Ibrahim, "A 5-D multi-stable hyperchaotic two-disk dynamo system with no equilibrium point: Circuit design, FPGA realization and applications to TRNGs and image encryption," *IEEE Access*, vol. 9, pp. 81352–81369, 2021.
[29] A. A. A. El-Latif, B. Abd-El-Atty, S. Elseuofi, H. S. Khalifa, A. S. Alghamdi, K. Polat, and M. Amin, "Secret images transfer in cloud system based on investigating quantum walks in steganography approaches," *Phys. A, Stat. Mech. Appl.*, vol. 541, Mar. 2020, Art. no. 123687.
[30] B. Abd-El-Atty, A. M. Iliyasu, H. Alaskar, and A. A. A. El-Latif, "A robust quasi-quantum walks-based steganography protocol for secure transmission of images on cloud-based E-healthcare platforms," *Sensors*, vol. 20, no. 11, p. 3108, May 2020.
[31] A. Sambas, M. Mamat, S. Vaidyanathan, M. Mohamed, W. M. Sanjaya, and Mujiarto, "A novel chaotic hidden attractor, its synchronization and circuit implementation," *WSEAS Trans. Syst. Control*, vol. 13, pp. 345–352, 2018.
[32] M. Chen, Z. Wang, F. Nazarimehr, and S. Jafari, "A novel memristive chaotic system without any equilibrium point," *Integration*, vol. 79, pp. 133–142, Jul. 2021.
[33] Y. Wu, C. Wang, and Q. Deng, "A new 3D multi-scroll chaotic system generated with three types of hidden attractors," *Eur. Phys. J. Special Topics*, vol. 230, nos. 7–8, pp. 1863–1871, Aug. 2021.
[34] *True Color Kodak Images*. Accessed: Aug. 3, 2021. [Online]. Available: http://r0k.us/graphics/kodak/
[35] A. Alanezi, B. Abd-El-Atty, H. Kolivand, A. A. A. El-Latif, B. A. El-Rahiem, S. Sankar, and H. S. Khalifa, "Securing digital images through simple permutation-substitution mechanism in cloud-based smart city environment," *Secur. Commun. Netw.*, vol. 2021, pp. 1–17, Feb. 2021.
[36] N. Tsafack, S. Sankar, B. Abd-El-Atty, J. Kengne, K. C. Jithin, A. Belazi, I. Mehmood, A. K. Bashir, O.-Y. Song, and A. A. A. El-Latif, "A new chaotic map with dynamic analysis and encryption application in Internet of Health Things," *IEEE Access*, vol. 8, pp. 137731–137744, 2020.
[37] T. Nestor, N. D. Dieu, K. Jacques, E. Yves, A. Iliyasu, and A. A. El-Latif, "A multidimensional hyperjerk oscillator: Dynamics analysis, analogue and embedded systems implementation, and its application as a cryptosystem," *Sensors*, vol. 20, no. 1, p. 83, Dec. 2019.
[38] Z. Hua, Y. Zhou, C.-M. Pun, and C. L. P. Chen, "2D Sine Logistic modulation map for image encryption," *Inf. Sci.*, vol. 297, pp. 80–94, Mar. 2015.
[39] Z. Hua, Y. Zhou, and H. Huang, "Cosine-transform-based chaotic system for image encryption," *Inf. Sci.*, vol. 480, no. 1, pp. 403–419, Apr. 2019.
[40] Y. Zhou, L. Bao, and C. P. Chen, "A new 1D chaotic system for image encryption," *Signal Process.*, vol. 97, no. 11, pp. 172–182, 2014.
[41] Y. Xian and X. Wang, "Fractal sorting matrix and its application on chaotic image encryption," *Inf. Sci.*, vol. 547, pp. 1154–1169, Feb. 2021.
[42] S. Askar, A. Karawia, A. Al-Khedhairi, and F. Al-Ammar, "An algorithm of image encryption using logistic and two-dimensional chaotic economic maps," *Entropy*, vol. 21, no. 1, p. 44, Jan. 2019.
[43] X. Wang and S. Gao, "Image encryption algorithm based on the matrix semi-tensor product with a compound secret key produced by a Boolean network," *Inf. Sci.*, vol. 539, pp. 195–214, Oct. 2020.
[44] Z.-H. Gan, X.-L. Chai, D.-J. Han, and Y.-R. Chen, "A chaotic image encryption algorithm based on 3-D bit-plane permutation," *Neural Comput. Appl.*, vol. 31, no. 11, pp. 7111–7130, 2018.
[45] X. Wang, L. Feng, and H. Y. Zhao, "Fast image encryption algorithm based on parallel computing system," *Inf. Sci.*, vol. 486, pp. 340–358, Jun. 2019.
[46] A. A. A. El-Latif, B. Abd-El-Atty, A. Belazi, and A. M. Iliyasu, "Efficient chaos-based substitution-box and its application to image encryption," *Electronics*, vol. 10, no. 12, p. 1392, Jun. 2021.

SUNDARAPANDIAN VAIDYANATHAN received the D.Sc. degree in electrical and systems engineering from Washington University in St. Louis, St. Louis, MO, USA, in 1996. He is currently a Professor and the Dean of the Research and Development Centre, Vel Tech University, Chennai, India. He has published over 550 Scopus-indexed research publications. His current research interests include linear and nonlinear control systems, chaotic and hyperchaotic systems, circuits, intelligent control, optimal control, mathematical modeling, and scientific computing.

ACENG SAMBAS received the Ph.D. degree in mathematics from Universiti Sultan Zainal Abidin (UniSZA), Malaysia, in 2020. He has been a Lecturer with the Muhammadiyah University of Tasikmalaya, Indonesia, since 2015. His current research interests include dynamical systems, chaotic signals, electrical engineering, computational science, signal processing, robotics, embedded systems, and artificial intelligence.

ESTEBAN TLELO-CUAUTLE received the B.Sc. degree from the Instituto Tecnológico de Puebla México, in 1993, and the M.Sc. and Ph.D. degrees from the Instituto Nacional de Astrofísica, Óptica y Electrónica (INAOE), México, in 1995 and 2000, respectively. In 2001, he was appointed as a Professor and a Researcher of INAOE. He has authored five books, edited 11 books, and around 300 works published in book chapters, international journals, and conferences. His research interests include analog signal processing, synthesis and design of integrated circuits, optimization by metaheuristics, design and applications of chaotic systems, security in the Internet of Things, symbolic analysis, and analog/RF and mixed-signal design automation tools. He serves as an Associate Editor for IEEE Transactions on Circuits and Systems—I: Regular Papers, *Engineering Applications of Artificial Intelligence*, *International Journal of Circuit Theory and Applications*, *Electronics*, *Integration, the VLSI Journal*, and *Frontiers of Information Technology and Electronics Engineering*.

AHMED A. ABD EL-LATIF received the B.Sc. degree (Hons.) in mathematics and computer science and the M.Sc. degree in computer science from Menoufia University, Egypt, in 2005 and 2010, respectively, and the Ph.D. degree in computer science and technology from the Harbin Institute of Technology (HIT), Harbin, China, in 2013. He is currently an Associate Professor of computer science with Menoufia University, Egypt, and the School of Information Technology and Computer Science, Nile University, Egypt. He has many collaborative scientific activities with international teams in different research projects. He has authored and coauthored more than 140 papers, including refereed IEEE/ACM/Springer/Elsevier journals, conference papers, and book chapters. His research interests include multimedia content encryption, secure wireless communication, the IoT, applied cryptanalysis, perceptual cryptography, secret media sharing, information hiding, biometrics, forensic analysis in digital images, and quantum information processing. He is a fellow of the Academy of Scientific Research and Technology, Egypt. He received many awards, the State Encouragement Award in Engineering Sciences 2016, Arab Republic of Egypt, the Best Ph.D. Student Award from the Harbin Institute of Technology, China, in 2013, and the Young Scientific Award, Menoufia University, Egypt, in 2014. He is an Associate Editor of *Journal of Cyber Security and Mobility* and *IET Quantum Communication*. He also leading many special issues in several SCI/EI journals.

BASSEM ABD-EL-ATTY received the B.S. degree in physics and computer science, the M.Sc. degree in computer science, and the Ph.D. degree in computer science from Menoufia University, Egypt, in 2010, 2017, and 2020, respectively. He is currently an Assistant Professor with the Faculty of Computers and Information, Luxor University, Egypt. He has authored and coauthored more than 30 papers, including refereed articles published by IEEE, Elsevier and Springer journals, conference papers, and book chapters. His research interests include quantum information processing and image processing. He is a reviewer in a set of reputable journals in Elsevier and Springer.

OMAR GUILLÉN-FERNÁNDEZ received the bachelor's degree from the Instituto Tecnológico de Veracruz, in 2015, and the M.Sc. degree in electronics from the Instituto Nacional de Astrofísica, Óptica y Electrónica (INAOE), México, in 2018, where he is currently pursuing the Ph.D. degree. He has published two books, two book chapters, two conferences, and 14 research articles. His research interests include chaotic systems, synchronization techniques, security of data transmission, embedded systems, and integrated circuit design and applications.

KHALED BENKOUIDER received the M.S. degree in automatic control and the Ph.D. degree from the University of Jijel, Jijel, Algeria, in 2015 and 2021, respectively. His M.S. research was on secure communications based on chaotic systems. His main research interests include dynamical systems, control systems, delayed systems, LPV systems, and chaotic systems synchronization.

MOHAMAD AFENDEE MOHAMED (Associate Member, IEEE) received the Ph.D. degree in mathematical cryptography from Universiti Sultan Zainal Abidin, in 2012. He currently serves as an Associate Professor for Universiti Sultan Zainal Abidin. His research interests include both theoretical and application issues in the domain of data security, and mobile and wireless networking.

MUSTAFA MAMAT received the Ph.D. degree from UMT, in 2007, with specialization in optimization. He was first appointed as a Lecturer with Universiti Malaysia Terengganu (UMT), in 1999. Later on, he was appointed with UMT as a Senior Lecturer, in 2008, and then as an Associate Professor, in 2010. He has been a Professor and the Dean of the Graduate School, Universiti Sultan Zainal Abidin (UniSZA), Malaysia, since 2013. To date, he has successfully supervised more than 60 postgraduate students and published more than 150 research papers in various international journals and conferences. His research interests include conjugate gradient methods, steepest descent methods, Broydens family, and quasi-Newton methods.

MOHD ASRUL HERY IBRAHIM was born in Kelantan, Malaysia. He received the B.Sc. degree in financial mathematics and the M.Sc. degree in applied mathematics from Universiti Malaysia Terengganu, Malaysia. He is currently pursuing the Ph.D. degree major in mathematical sciences with Universiti Sultan Zainal Abidin. He is also working as a Senior Lecturer with Universiti Malaysia Kelantan and the Director of the Publication and Rating Division. His current research interests include optimization, numerical analysis, business mathematics, and business statistics. He writes regularly and has published more than 50 scientific articles in journals and conferences.